Wroclaw University of Science and Technology

Faculty of Fundamental Problems of Technology

Department of Experimental Physics

Laboratory for Optical Spectroscopy of Nanostructures

Joanna Jadczak

Summary of professional accomplishments

Wrocław 2019

1. Name:

Joanna Natalia Jadczak

2. Degrees and diplomas

2012

Doctor of Physics, Wroclaw University of Science and Technology, Faculty of Fundamental Problems of Technology, Department of Experimental Physics
Thesis subject: *Magneto-optical spectroscopy studies of positively charged excitons in two- dimensional semiconducting nanostructures.*
Degree cum laude.
Advisor: dr hab. Leszek Bryja

2008

Master of Science, Wroclaw University of Science and Technology, Faculty of Fundamental Problems of Technolog
Supervisor: dr hab. Leszek Bryja

3. Employment in scientific institutions:

October 2015 -present

Assistant Professor at Wroclaw University of Science and Technology, Faculty of Fundamental Problems of Technology, Department of Experimental Physics

January -July 2014

Post-doctoral internship in Department of Electronic and Computer Engineering, National Taiwan University of Science and Technology, Taipei, Taiwan

February- December 2013

Post-doctoral internship in Laboratoire National des Champs Magnétiques Intenses, Toulouse, France

September 2012 -2015

Assistant at Wroclaw University of Science and Technology, Faculty of Fundamental Problems of Technology, Institute of Physics

Other short-term scientific internships:

- Internships at Technical University Dortmund (Germany) in Experimentalle Physik II group of Prof. Manfred Bayer: February 2019, November 2016, May 2012, February and December 2011, April 2010.
- Internships in National High Magnetic Field Laboratory, Grenoble: Novemeber and June 2008, October 2009, October 2011.
- Interships in Department of Electronic and Computer Engineering, National Taiwan University of Science and Technology, Taipei, Taiwan: July, October 2018

4. Scientific achievements * resulting from art. 16 sec. 2 of the Act of 14 March 2003 on academic degrees and academic title and on degrees and title in the field of art (Journal of Laws No. 65, item 595, as amended):

A) Title of scientific achievement

The nature of excitonic complexes and lattice dynamics in two- dimensional transition metal dichalcogenides.

B) List of publications constituting a scientific achievement (ordered from the newest to the oldest):

[H1] **J. Jadczak**, L. Bryja, J. Kutrowska-Girzycka, P. Kapuściński, M. Bieniek, Y.S. Huang, P. Hawrylak, *Room temperature multi-phonon upconversion photoluminescence in monolayer semiconductor WS_2*, Nature Communications **10**, Article number: 107 (2019), IF 12.353

[H2] **J. Jadczak**, J. Kutrowska-Girzycka, T. Smoleński, P. Kossacki, Y. S. Huang, and L. Bryja, *Exciton binding energy and hydrogenic Rydberg series in layered ReS_2*, Scientific Reports 9, 1578 (2019) IF 4.122

[**H3**] J. Kutrowska-Girzycka, **J. Jadczak**, L. Bryja, *The study of dispersive 'b'-mode in monolayer MoS_2 in temperature dependent resonant Raman scattering experiments*, Solid State Communications, Volume **275**, July 2018, Pages 25-28, IF **1.549.**

[H4] **J. Jadczak**, *Photoluminescence studies of excitonic complexes in atomically thin $Mo(S_ySe_{1-y})_2$ Alloys*, Acta Physica Polonica A **132**, 307 (2017), IF **0.857**

[H5] **J. Jadczak**, A. Delgado, L. Bryja, Y. S. Huang, P. Hawrylak, *Robust high-temperature trion emission in monolayers of $Mo(S_ySe_{1-y})_2$ alloys*, Phys. Rev. B, Volume **95**, Article number: 195427 (2017), IF **3,836**

[H6] **J. Jadczak**, J. Kutrowska-Girzycka, P. Kapuściński, Y.-S. Huang, A. Wójs, L. Bryja, *Probing of free and localized excitons and trions in atomically thin WSe_2, WS_2, $MoSe_2$ and MoS_2 in photoluminescence and reflectivity experiments*, Nanotechnology, Volume **28**, Article number: 395702 (2017), IF **3.404**

The following cycle of literature designations has been adopted:
- own works constituting a scientific achievement are marked with the letter H, e.g. [H1]
- own works directly related to the subject of scientific achievement are marked with the letter B, e.g. [B1]
- own work other, not related to the subject of scientific achievement, are marked with the letter I, e.g. [I1]
- quoted works of other authors are marked without the use of letters, e.g. [1].

C) Description of a scientific goal of aforementioned works and the results achieved including a discussion of their potential applications.

Abstract

The series of articles is devoted to discussion of the fundamental physical properties of the monolayer binary and ternary group-VI transitional metal dichalcegonides (TMDs) such as MoS_2, $MoSe_2$, WS_2, WSe_2 and $Mo(S_xSe_{1-x})_2$ and also of group VII such as ReS_2 crystals. The monolayer TMDs due to the coupling of the spin – valley degree of freedom, strong confinement of carriers to single layer and reduced dielectric screening provide a unique possibility to study many-body effects. Accordingly, my research are mainly focused on the electron – electron and electron – phonon interactions in two dimensional TMDs.

The electron – electron interaction studies were carried out in the comparative temperature –dependant (7- 295 K) photoluminescence (PL), photo excitation photoluminescence (PLE) and reflectance contrast (RC) measurements in monolayer group VI TMDs with high crystal symmetry [**H4**, **H5**, **H6**] and also in mono- and few layer VII group TMDs such as ReS_2 crystals, which possess reduced crystal symmetry and in-plane anisotropy of the optical properties [**H2**]. Based on the optical spectra I analyzed different excitonic complexes which were characterized in terms of their binding energies, total charge, form of localization and spin –valley configuration of the constituent carriers. In the PL and Raman scattering investigations I showed, that the binding energy of an additional electron to the neutral exciton is comparable with a phonon energy. Then, I demonstrated that strong increase of trion PL intensity with the increase of sulfur mole content in ternary $Mo(S_ySe_{1-y})_2$ is attributed to two effects: (i) strong increase of exciton - trion coupling mediated by the optical phonon, which is realized by tuning phonon energy through trion binding energy, and (ii) significant increase of two-dimensional electron gas concentration [**H4, H5**]. Furthermore, I showed that strong exciton – phonon coupling in monolayer TMDs leads to the high energy, multi- phonon upconversion photoluminescence, which may be used in the laser cooling [**H1**]. In the reverse PL measurements in monolayer WS_2, I showed that upconversion photoluminescence energy gain is up to 150 meV at T = 295 K and 42 meV at T = 7 K. In addition, I showed that upconversion mechanism strongly depends on two electron concentration (2DEG), which was demonstrated in power- dependant anti-Stokes excitonic emission measurements performed in ambient and in vacuum [**H1**]. The strong impact of 2D carrier concentration on the electron- phonon interaction was also probed in the resonant Raman scattering measurements in monolayer MoS_2. I showed that dispersion of *b* mode strongly depends on 2DEG concentration, which was tuned by the change of environmental conditions. In addition, I confirmed that it is the second order scattering process involving combinations of the acoustic LA and TA phonons at K points of BZ [**H3**].

Presented results are important not only from the fundamental point of view but also can be consider in applications. They highlight the impact of environmental conditions, chosen substrate and structural defects on optical properties of monolayer TMDs.

State of knowledge before the beginning of the studies and discussion of the scientific purpose of the research

Semiconducting transition metal dichalcogenides (TMDs) of chemical formula MX_2 (such as WSe_2, WS_2, $MoSe_2$ and MoS_2) have attracted considerable attention from the scientific community due to the underlying physics and promising applications in photonics, optoelectronics and the development of valleytronics [**1-12**]. These layered materials are indirect semiconductors in bulk form, but when thinned down to one monolayer they become direct semiconductors in the visible to the near infrared region of the optical spectrum [**1-12**]. The bulk crystals are built up of van-der-Waals bonded X- M -X units which consist of two hexagonal planes of X atoms and an intermediate hexagonal plane of M atoms coordinated through covalent interactions with the S atoms in a trigonal prismatic arrangement. In monolayers of TMDs the bottom of the conduction band and the top of the valence band are located at the binary indexed corners K^+ and K^- of the 2D hexagonal Brillouin zone. The lack of inversion symmetry and a strong spin–orbit coupling in single layers of TMDs results in valley-contrasting strong spin splitting of the valence and conduction bands. The confinement to a single layer and reduced dielectric screening lead to strong many body effects mediated by Coulomb interactions. The optical spectra of TMDs monolayers are dominated by excitons, bound electron–hole pairs (X = e + h), which exhibit very high binding energies of a ~500 of meV [**13-15**], leading to their stability at room temperature. In the optical spectra of TMDs monolayers also different excitonic complexes are observed. In the presence of excess carriers charged excitons, called trions (T), consisting of two electrons and one hole (X^- = 2e + h) or two holes and one electron (X^- = 2e + h), are detected in optical spectra of TMD monolayers. The binding energy of an additional carrier to neutral exciton is determined in the optical spectra as an energy distance between neutral and charged excitons and it varies from 30 to 42 meV [**16-27, H4-H6**]. Varying values of trion binding energies for particular TMDs monolayers are related to the different doping level and different position of Fermi level [**22**].

The spin splitting of the valence band Δv, leading to formation of so called A and B excitons, amounts to about 150, 180, 430, and 450 meV for the MoS_2, $MoSe_2$, WS_2, and WSe_2 monolayer, respectively [**28**]. As predicted in theoretical calculations [**6**, **29**], the conduction-band spin splitting Δ_c is significantly smaller and shows a larger relative variance between different TMDC monolayers. It leads to the splitting between the dark and bright exciton subbands of the so-called A-exciton defined by the spin–orbit splitting in the conduction band, Δc. Bright excitons are composed of an electron and hole with parallel spin, whereas dark excitons are composed of the electron and hole with the opposite spin. In molybdenum based TMDC Δ_c is predicted to be positive (equals 3 and 21 meV in MoS_2 and $MoSe_2$, respectively), resulting in the lowest energy exciton subband being bright. In contrast, in tungsten based TMDC Δ_c is predicted to be negative (equals -32 and -37 meV in WS_2 and WSe_2, respectively), and the lowest energy subband is dark [**29**]. This leads to the significant differences observed in the emission spectra of molybdenum and tungsten based compounds which, among others, are related to the detection of different spin - valley configurations of negative trion [**24**, **26**]. In the low temperature photoluminescence (PL) spectra of $MoSe_2$ monolayers, well resolved exciton and trion transitions, separated by 30 meV, are detected [**20, 21, H4-H6**]. While, low temperature emission spectra of WSe_2 are dominated additionally by lines positioned in the low energy sector of PL spectra [**17-19**]. The nature of these lines is still under debate. They have been assigned to excitons localized on defects (L) [**17**] or phonon- assisted transitions [**29**]. There is al-

so another interpretation based on low temperature power dependent PL experiments reported on observation of biexciton emission (XX) among these spectral lines [**25**]. On the other hand, similar investigations conducted on WS_2 monolayers force the interpretation, that the XX emission is merged with the emission of a localized exciton (L) [**23**], which is based on a linear increase in the integrated XX/L PL intensity for low excitation densities and a quadratic one for higher exciton densities. Moreover, other authors reported investigations in favor of a trion nature of this species [**26**]. They showed in PL experiments on a WSe_2 monolayer that by applying a gate voltage, the spectral weight of PL transfers from the neutral exciton (X) to the trion (T) and at a voltage higher than 20 V, to a new PL feature (named X_2'), positioned at the same energy as the biexciton emission.

The aim of my investigations was to gain insight into the nature of excitonic complexes observed in different energy regions of the optical spectra of two dimensional group-VI and -VII TMDs. For this purpose, I constructed an experimental set- up, which allowed me to conduct the simultaneous reflectance contrast (RC), photoluminescence (PL), excitation photoluminescence (PLE) and Raman scattering measurements with a micrometric spatial resolution in broad temperature range from 7 to 300 K. I also developed a method of monolayer separation based on mechanical exfoliation from bulk crystals using different adhesion tapes and elastomers. On the base of experimental results I analyzed all the observed excitonic complexes and I interpreted them in terms of their binding energies, total charge, form of localization and spin - valley configuration of the constituent carriers. I also studied many-body effects related to electron – phonon interactions.

Achieved scientific results being the subject of habilitation and prospects for their possible use.

1) Probing the nature of the excitonic compexes in monolayer WSe_2, WS_2, $MoSe_2$ and MoS_2.

In the work [**H6**], based on the comparative temperature- dependant photoluminescence (PL) and reflectance contrast (RC) experiments I discussed the optical properties of WSe_2, WS_2, $MoSe_2$ i MoS_2 monolayers. In order to characterize all the monolayers under the same condition, including the impact of the substrate on the optical properties, they were exfoliated onto the same target SiO_2/Si substrate. In figure 1.1 (a)- (d) examples of comparative PL and RC spectra of all the studied monolayers are presented at T = 7 K. Two resonances are observed in the higher energy region of the PL and RC spectra for all the samples. They are attributed to the optical transitions of an exciton (X, a higher-energy one) and trion (T, a lower-energy one). The common feature observed in the PL spectra of all the studied monolayers is that the PL intensity of the trion exceeds that of the exciton. In contrast, the RC spectra are much more diverse. In reflectivity spectra of selenides, WSe_2 and $MoSe_2$, the exciton resonance is substantially stronger than that of the trion. Moreover, in WSe_2 the trion resonance is scarcely distinguished in the RC spectra. In the RC spectra of WS_2 the X resonance is slightly stronger than the T resonance, and only in MoS_2 the T resonance is stronger than that of X. The reason

for the difference in the optical amplitude of the exciton and trion in the PL and RC spectra is that the strength of the exciton and trion resonances in reflectivity is determined by respective density of states, whereas the PL intensity is contributed additionally by a state occupation factor. The qualitative comparison of the optical properties shows that the relation in the strength of the exciton and trion resonances in the RC spectra depends on the two dimensional carrier concentration (2DCG), which in sulfides is about two orders of magnitude higher than in selenides [**4, 16**].The increase in the 2DCG concentration results in the increase in the strength of the trion resonance relative to the strength of the exciton resonance.
An inspection of the RC spectra presented in Fig. 1.1 shows that the highest 2DCG concentration (electron) is expected in MoS_2, then in WS_2, next in $MoSe_2$, whereas the lowest in WSe_2. This qualitative estimation of the 2DCG concentration turned out to be very supportive, particularly for the interpretation of the mentioned series of emission lines observed in the low energy sector of the PL spectra of the tungsten compounds [**17, 25**].
In the work [**H6**], in the low energy sector of the PL spectra of the WSe_2 and WS_2 MLs shown in figures 1. 1 (a) and (b) a group of high intensity lines, labeled by analogy to localized excitons as (L_1–L_n) is detected. As clearly seen in Fig. 1(a), none of the (L_1–L_n) lines are individually distinguishable in the RC spectra of WSe_2. However, it is significant that in the RC spectra of WS_2 a new additional line (named L0) is observed. Interestingly, its energy position in the RC spectra matches the energy of the prominent emission line L_1, which was interpreted previously as biexciton (XX) [**23**]. At that stage of investigation, according to my knowledge, it was first observation of the L_0 resonance in RC spectra of the WS_2.

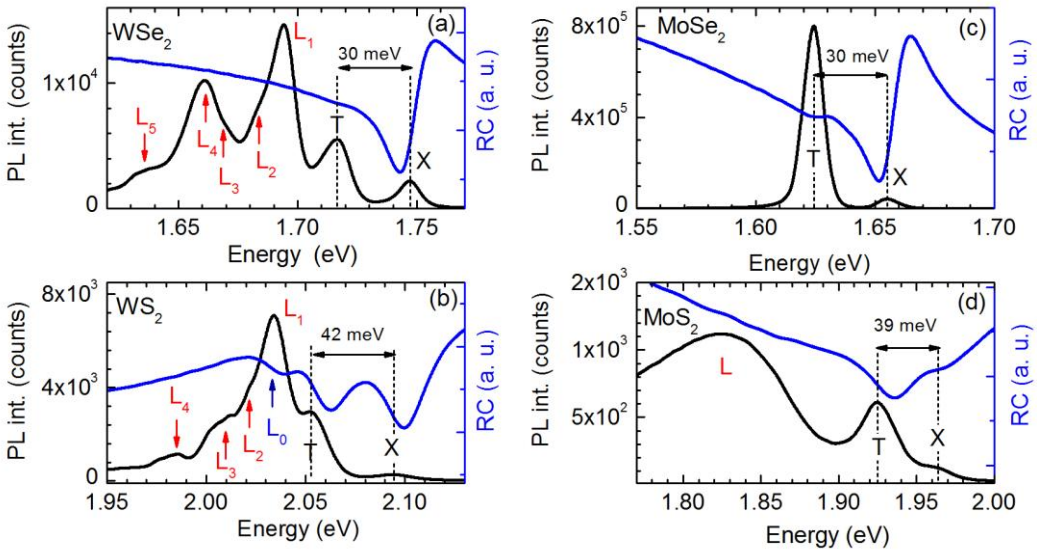

Fig. 1.1 Examples of comparative PL and RC spectra recorded at T = 7 K for the monolayers of: (a) WSe_2, (b) WS_2, (c) $MoSe_2$, (d) MoS_2.

Further investigation of RC spectra showed that the strength of the L_0 resonance is strongly position dependent and there is a clear correlation between the strength of

the X, T and L_0 resonances. In figure 1.2 the RC spectra of the WS_2 monolayer recorded at different points on the monolayer are presented. The increase in the strength of the L_0 resonance is accompanied by the simultaneous increase in the strength of the T resonance and the decrease of the strength of the X resonance. Since the increase in the trion strength relative to the exciton strength is related to the increase in the 2DCG concentration, this observation implies that: (1) the concentration of the 2DCG is different in different regions of the studied WS_2 monolayer, and (2) the strength of the L_0 resonance increases with the increase in the 2DCG concentration. The observed increase in the strength of the T and L_0 resonances in the RC spectra with the increase in the 2DCG concentration allowed me to assess both features as related to the fine structure of the trion.

It is well established from the PL studies of gated WS_2 structures that pristine WS_2 MLs are n-type doped, so I attribute the T and L_0 resonances to two optically bright negatively charged trion species (X^-). Due to the Pauli principle two constituent electrons in a trion in TMDC monolayers occupy states with different spin or valley index. In a WS2 monolayer this leads to three possible pairs of doubly degenerate configurations of the bright trion X^- complex, schematically presented in Fig. 1.3 (a) – (c): (a) the intravalley trion, with a hole and a pair of electrons in the same valley in the upper and lower conduction bands, forming an electron spin singlet state, (b) the intervalley trion, with electrons located in different valleys, in the upper and lower conduction bands, forming an electron spin triple state, and (c) the intervalley trion with electrons located in different valleys, but in the upper conduction bands, forming an electron singlet state.

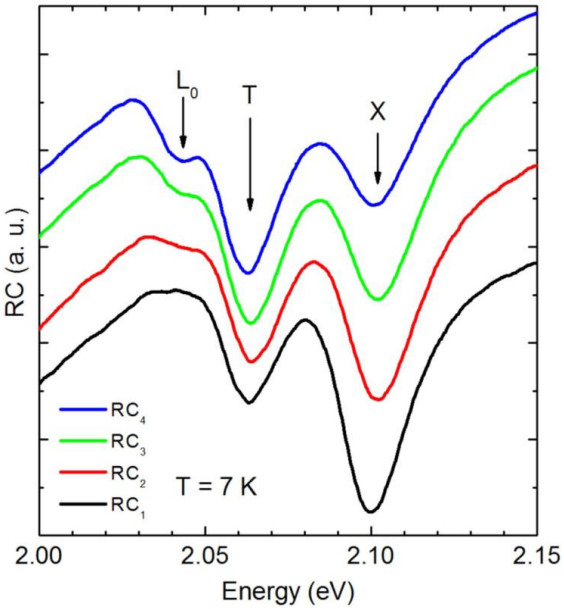

Fig. 1.2 The RC spectra of WS_2 recorded at different points on a monolayer.

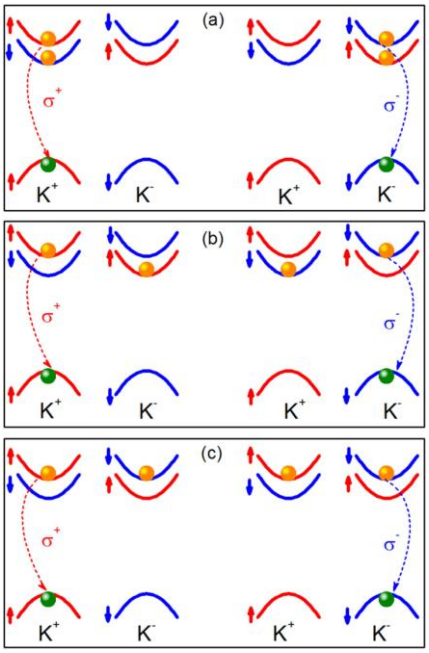

Fig. 1. 3 A schematic illustration of possible configurations of a hole and a pair of electrons in trion in a WS_2 monolayer

The formation of trion complexes with an additional electron in the lower-energy spin-split conduction band, presented in figures 1.3 (a) and (b), are more probable at low two-dimensional electron gas (2DEG) concentrations, whereas the formation of the trion complex with electrons in the higher-energy spin-split conduction bands are preferable at higher 2DEG concentrations, when the electron Fermi level is located above the upper spin-split conduction band.

One possible model that could explain the coexistence of the T and L_0 resonances in the RC spectra is that the WS_2 monolayer is inhomogeneous, possibly due to interaction with the substrate or randomly created vacancies which act as acceptors or donors, resulting in regions with low and high 2DEG concentration.

The proposed interpretation of the fine structure of the trion in WS_2 monolayer predicts energy splitting of the trion into three separate resonances, not resolved within the linewidth of the T and L_0 features in RC spectra. The observation of the splitting of the T feature into two components, attributed to the electron spin singlet (T_S) and triplet states (T_T), with an additional electron in the lower conduction band [**24**], is very difficult in the optical spectra of the standard WS_2/SiO_2 structures due to small splitting of the singlet–triplet states (7 - 11 meV) in comparison to the linewitdh of the T resonance. However, it can be achieved in the high quality WS_2/hBN/SiO_2/Si structures [**H1**].

To gain more insight into the character of the L_1 and other low energy L lines I performed excitation power and temperature dependant PL measurements of WS_2 and WSe_2 monolayers. At T = 7 K and low excitation powers all the X, T and L lines in the PL spectra of WSe_2 and WS_2 are well separated and have comparable intensities, whereas at higher excitation powers the L_1 line strongly dominates the spectra. It is worth to note, that in the emission spectra of WSe_2 the L_1 and L series were better resolved than in the emission spectra of WS_2. However, the same relation in the evolution of the total PL intensity of the X, T, L_1 and L_2–L_4 species as a function of the excitation power were observed. I showed that the integrated PL intensity of the exciton and trion grows almost linearly, whereas the integrated PL intensity of the L_1 exhibits superlinear growth with the excitation power. The lines L_2–L_5 in WSe_2 and L_2–L_4 in WS_2 grow sublinearly with the excitation power. To compare my data with the previous reports [**23**, **25**] I analyzed the emission from the L_1 in terms of the neutral exciton X strength using a power law relation of the form $I_{L1} \sim I_X^{\alpha}$. For WSe_2 I obtained $\alpha = 1.28$, slightly lower than $\alpha = 1.39$ obtained in [**25**]. For WS_2 I obtained $\alpha = 1.46$, whereas in [**23**] authors reported on a linear dependence of the total PL intensity of the relevant line for low excitation powers and a quadratic one for higher excitation powers. They interpreted this effect as related to emission of two different species with the same PL energy: at low excitation power the main contribution to PL stems from defect bound excitons, whereas for higher excitation powers the emission from biexciton dominates. Although the relation of the L_1 feature in PL spectra of WSe_2 and WS_2 to biexciton emission, proposed in the previous studies, is convincing, on the base of my study of the PL and RC spectra of WS_2 monolayer I proposed an alternative interpretation of the L_1 feature as related to the superposition of: defect bound exciton, trion emission

and biexciton. However, it is worth to note that the simultaneous observation of all the excitonic complexes (particularly in WS_2) requires different experimental conditions, including different 2DCG concentration and different quality of the studied sample (highly or low defected). As was shown in theoretical calculations [**30**, **B2**], point defects in TMDs serve as both, donors or acceptors. In strongly confined systems, by analogy to 2D GaAs/$Al_xGa_{1-x}As$ structures, in the presence of an excess electron (hole) gas, a neutral donor, D_0 (or a neutral acceptor, A^0) can bind an additional electron (hole) to form a charged complex D^- (or A^+) [**31**, **I1**, **I3**]. The stability of such charged complexes is also expected in TMDC monolayers. Moreover, as predicted in theoretical calculation, their binding energy is equal to about 30 meV [**32**]. Hence, in a highly n-type doped WS_2 monolayer the formation of optically active complex of an exciton bound on a negatively charged donor (D^-X = = D^0 + e +e +h) is very probable, but its contribution to the PL spectra is excepted to be very weak. Another scenario, possible in the defected structure, is that the L_1 feature is additionally contributed by emission of excitons bound on neutral donors or acceptors (D^0X = D^0 + e+ h or A^0X = D^0 + e+ h). It is well known from the PL studies of bulk crystals [**33**, **34**] that the D^0X and A^0X emission intensities exhibit superlinear dependence on the laser power, and the similar behavior is expected in atomically thin TMDC. Consistently, I attributed the L_2–L_4 lines positioned in the PL spectra of WS_2 at lower energies in respect to the L_0 line to optical transitions of: electron to acceptor (e–A^0), hole to donor (h–D^0), and donor to acceptor (D^0–A^0) complexes, as they exhibit similar sublinear growth of the emission strength as a function of the laser power as relevant complexes in bulk crystals [**33**, **34**].

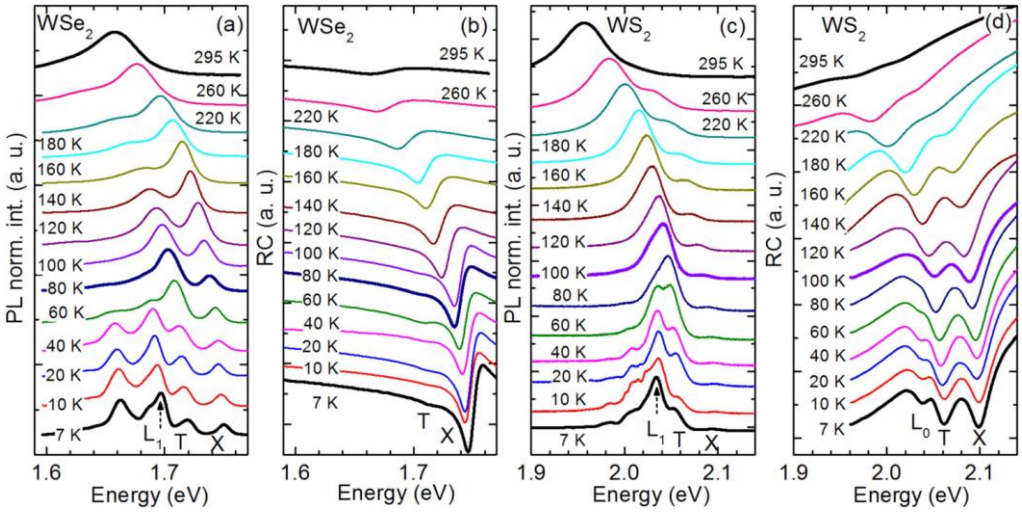

Fig. 1.4 The temperature evolution of the PL and RC spectra of WSe_2 and WS_2 monolayers. (a) PL spectra of WSe_2. (b) RC spectra of WSe_2. (c) PL spectra of WS_2. (d) RC spectra of WS_2.

The temperature dependant PL and RC studies of WSe_2 and WS_2 monolayers also support proposed interpretation of the L_0, L_1, L_2-L_n transitions. As seen in the PL

spectra presented in Fig. 1.4 (a) i 1.4 (c), with increasing temperature the low energy L peaks rapidly quench and they are not detected in the spectrum at temperatures above 80 K. This rapid quench of the low intensity lines is independent of the excitation power. However, in both monolayers with increasing temperature the PL intensity of the L_1 line decreases much slower than the PL intensity of the other L lines. Additionally, in the WS_2 monolayer the L_0 resonance in the RC spectra exhibits similar temperature evolution as the L_1 resonance in the PL spectra and disappears from the RC spectra at the same temperature T > 80 K. This accounts for the relation of the L_0 and L_1 resonance to the same radiative complex. In order to interpret the rapid temperature quenching of the L_0 and L_1 features I considered the impact of the inhomogeneous distribution of the 2DEG in the WS_2 monolayer. In other words, I assumed that due to the potential fluctuations in some regions of the monolayer the upper spin-split conduction band is positioned below the Fermi level. As the temperature increases, the access electrons become more mobile, that causes a more homogeneous redistribution of the 2DEG over the whole sample, which in turn leads to decrease of the number of electrons in the upper conduction bands and the L_0 resonance disappears from the RC spectra of the WS_2 monolayer. With the increase in the temperature, the occupation of the lower spin-split conduction band is only weakly affected and the T resonance, related to the trion complex with the access electron in the lower spin-split conduction band, is detected in the PL and RC spectra up to T = 295 K.

In contrast to low energy L lines the X and T lines contribute to the PL spectra of WS_2 and WSe_2 monolayers at all measured temperatures T= 7–295 K. This is related to a higher oscillator strength of the X and T states compared to the localized states. Additionally, the observation of the strong temperature induced transfer of the optical strength from the L features to the exciton (X) and trion (T) (Fig. 1.5) implies that the exciton and trion are related to essentially free states, for which localization has insignificant effect on the emission energy, whereas the L features are related to strongly localized states, positioned in the low energy sector of the emission spectra. The temperature quenching of L lines in emission spectra above 80 K can be explained by the fact that excitons gain kinetic energy and become less susceptible to the capture process.

Looking at the temperature evolution of the integrated PL intensities of excitons and trions in WSe_2, WS_2, $MoSe_2$ and MoS_2 monolayers presented in Fig. 1.5 (a) – (d), one can find significant differences between them, mainly related to the different 2DEG concentrations in sulfides and selenides and the opposite sign of the conduction band spin-splitting in the tungsten- and molybdenum based TMDs. In figure 1.6 the logarithm of the trion to exciton ratio of integrated PL intensity is drawn as a function of invert temperature in WS_2, WSe_2 and $MoSe_2$. In high temperature regime (different for individual TMDs), the temperature evolution of the total PL intensity of the trion and exciton lines can be described using the Boltzmann law: $\sim\exp-(E_T- E_X)/k_BT$, where E_T and E_X are the trion and exciton energy positions in the PL spectra, and k_B isthe Boltzman constant.

As is seen from Fig. 1.6, the ratio of the exciton to trion PL intensity obeys Boltzmann law in WSe_2 at temperatures above T > 80 K, when the L lines disappear from the PL spectra. Moreover, the energy $\Delta E = -(E_T - E_X) = 30$ meV obtained from the Boltzman law is in good agreement with the energy separation of the T and X lines in the PL spectra (Fig 1.1 (a)). In contrast, in WS_2, where the L lines disappear from the PL spectra in the same temperature range, the ratio of the exciton to trion PL intensity obeys Boltzmann law at much higher temperatures T > 180 K. Also, the energy $\Delta E = 46$ meV obtained from the Boltzman law is slightly higher than energy separation of the T and X lines in the PL spectra which is equal to 42 meV (Fig 1.1 (b)). In $MoSe_2$, where no additional lines, except X and T, are observed in the PL spectra, the Boltzman law for emission lines is valid at T > 60 K, when the trion PL intensity starts to decrease significantly. This result reveals a complex interplay between the effect of different recombination channels (radiative and non-radiative) and 2D carrier concentration in WSe_2, WS_2 i $MoSe_2$ monolayers. However, in high temperature regime, different for different samples, radiative recombination of the trion and exciton are the dominant recombination channels.

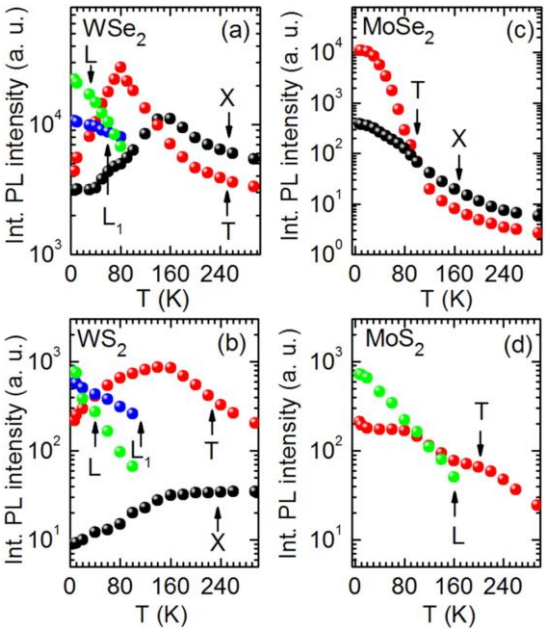

Fig. 1.5 Integrated PL intensities of excitons, trions and localized excitons as a function of the temperature in: (a) WSe_2, (b) WS_2 (c) $MoSe_2$ and (d) MoS_2.

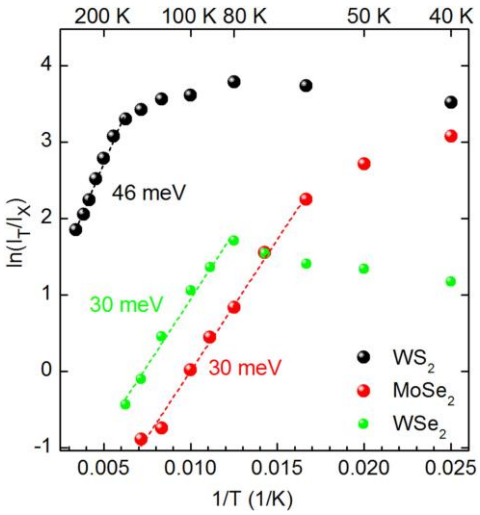

Fig. 1. 6 Integrated PL intensity rate $\ln(I_T/I_X)$ of the trion (T) and exciton (X) lines as a function of 1/T (symbols) for WS_2,WSe_2 and $MoSe_2$.

Significant difference in the energy separation of the trion and exciton lines in the PL spectra of selenides and sulfides are related to a strong difference in their 2D carrier concentration [**4, 16**]. In selenides, WSe_2 and $MoSe_2$, the carrier concentration is low and the energy separation of the X and T lines is equal to the trion binding energy. However, in WS_2 and MoS_2, the 2D electron concentration is high, which causes that during the radiative recombination of an electron– hole pair in a

trion complex, an additional electron is excited over the Fermi energy due to the space filling effect, and the relation between the exciton and trion positions in the PL spectra is given by the formula $\Delta E = E_b + E_F$ [**22**].

In order to determine the trion binding energy one has to decrease the 2D carrier concentration, what can be realized in a gated structure. Lacking capabilities to conduct transport measurements on the monolayers I performed the following additional PL experiments in ambient and in vacuum. It is well established that under ambient conditions the physisorbed O_2 and H_2O molecules deplete n-type materials such as MoS_2 and WS_2, much more than conventional electric field gating [**35**, **36**].

The comparison of the RC and PL spectra recorded at T = 295 K in ambient and vacuum conditions for all the studied monolayers is shown in Fig. . 1.7 (a)-1.7 (d). The experiments were performed under the same conditions for all the samples.

In the PL and RC spectra of selenides, WSe_2 and $MoSe_2$, recorded at T = 295 K, in ambient and in vacuum, only one line of the exciton is detected in both monolayers. The energy position of the X line in the PL and RC spectra in both monolayers is almost the same. This observation confirms that the 2DCG concentration is substantially lower in the selenides than in the sulfides.

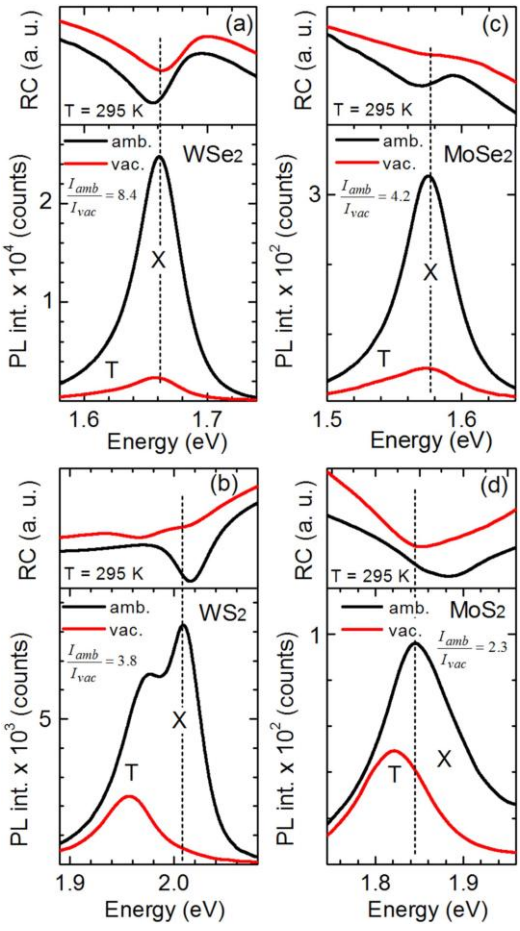

Fig. 1.7 The PL spectra recorded at T = 295 K in ambient (black line) and vacuum (red line) for (a) WSe_2, (b) WS_2, (c) $MoSe_2$ and (d) MoS_2.

In the sulfides, WS_2 and MoS_2, the shape and energy position of the PL lines and RC resonances strongly differ between experiments performed in ambient and vacuum, which confirms the previous reports that in ambient the 2DCG concentration is strongly depleted. The PL spectra of WS_2 and MoS_2 measured in vacuum are dominated by the trion. However, in the PL spectra of WS_2 measured in ambient well resolved peaks of X and T are resolved. Their energy separation equal to 30 meV is lower than the energy separation of the X and T peaks in PL spectra measured at low temperatures in vacuum which amounts 42 meV. Hence, the Fermi level can be evaluated using equation $E_F = \Delta E - E_b$ = 12 meV. This value is equal roughly to one half of theoretically predicted energy distance between spin-split conduction bands Δc, which means that Fermi level in WS_2/SiO2 structures is positioned between them. Then, using the equa-

tion $n = m_e E_F/\pi\hbar^2$ and the electron effective mass $m_e = 0.37$ [**6**], we calculate the intrinsic 2D electron concentration $n = 1.8 \times 10^{12}$ cm^{-2}. In the PL spectra of MoS_2 measured in ambient we detect only the T line, which enables us to evaluate the trion binding energy. This observation also shows the high 2D electron gas concentration in MoS_2, even in vacuum. Using the theoretically calculated trion binding energy in MoS_2 as $E_b = 30$ meV [**32**] and the electron effective mass of $m_e = 0.35$ [**37**] and also $\Delta E = 43$ meV we evaluate the Fermi energy as $E_F = 13$ meV and the intrinsic 2D electron concentration as $n = 1.9 \times 10^{12}$ cm^{-1}. These calculations confirm previous qualitative estimation of 2DEG concentration in the monolayer TMDs, which was proposed on the grounds of the comparative RC measurements.

2) Phonon assisted upconversion photoluminescence processes in WS_2 and WS_2/hBN heterostructures.

The atomically thin semiconductors based on transition metal dichalcogenides due to their very strong photon–exciton [**1 -15**] and and phonon–exciton interactions [**29**, **H5**] are very promising for applications based on the anti – Stokes processes in which an absorption of a photon leads to reemission of a photon at energy higher that the excitation energy [**38**, **39**]. Moreover, tungsten- based TMDs appear to be particularly effective due to prominent emission intensity in ambient, about two orders of magnitude higher than in molybdenum- based compounds [**H6**].

Recently, Jones et al.[**38**] reported phonon-mediated upconversion of photon emission by ~30 meV up to 250 K, from trion ($T = X^-$) to exciton (X), in a single layer of WSe_2. This was possible because the strong confinement of carriers to a single layer results in a very high binding energy of an electron to an exciton forming a trion, ~30 meV, comparable with a phonon energy [**38**, **40**].

The motivation for my studies of the exciton complex- phonon interactions was based on the comparable values of the energy separation of the X and T lines in PL spectra of monolayer TMDs [**H5**, **H6**] with the energies of optical phonons, such as: $\Delta E = 30$ meV and $E_{A1} = 29.8$ meV for $MoSe_2$[**40, H4**], $\Delta E = 39$-43 meV and $E_{A1} = 50$ meV for MoS_2 [**40, H4**], $\Delta E = 43$ meV and $E_{A1} = 52$ meV for WS_2 [**40**, **B5**]. Taking into account both the phonon energy and efficiency of the emission intensity in different TMDs in ambient [**H6**], I chose monolayer WS_2 for further investigations.

In contrast to ref. [**38**], I demonstrated a room temperature upconversion photoluminescence process in a monolayer semiconductor WS_2 with a larger energy gain, up to 150 meV. I also showed that the energy gain significantly depends on the temperature and increases from 42 meV at 7 K to 150 meV at 295 K.

Since the optical properties of WS_2 monolayer related to relative X and T PL intensities are strictly influenced by the temperature, environment and target substrate, the studies were started with comparing the upconversion photoluminescence process in WS_2/SiO_2 and WS_2/hBN/SiO_2/Si structures under ambient conditions.

For both structures, the incident photons (1. 85 eV) are converted into emitted photons with an energy higher by 150 meV, even though the intensity of the upconversion emission detected in WS_2/hBN/SiO_2/Si heterostructure is one order of magnitude lower than in WS_2 deposited directly on the SiO_2/Si substrate.

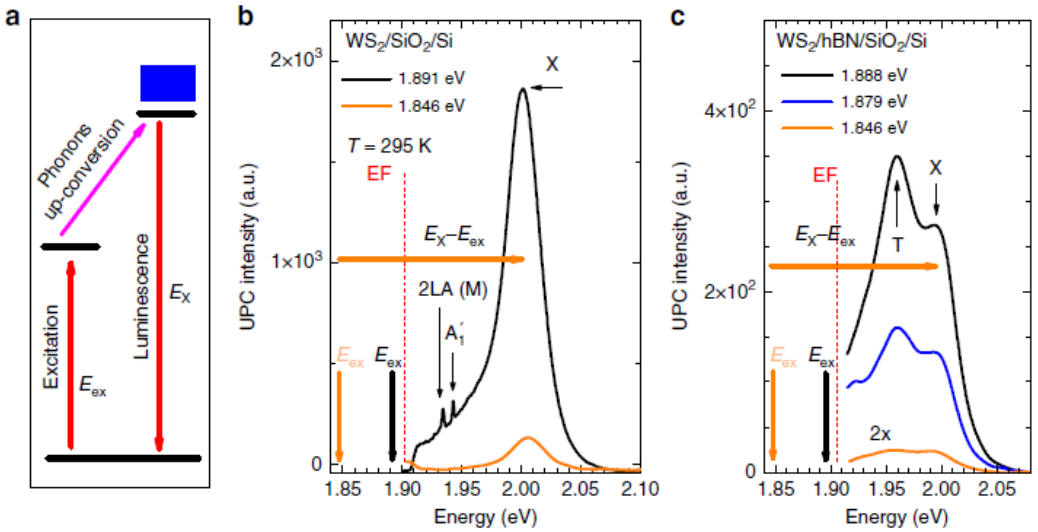

Fig. 2.1 Upconversion photoemission process in monolayer WS_2. (a) The schematic representation of upconversion process. (b) Examples of the upconversion photoemission spectra in WS_2/SiO_2/Si recorded for different excitation photon energies. (c) Examples of the upconversion photoemission spectra in WS_2/hBN(136 nm)/SiO_2/Si detected for different excitation photon energies. To reduce laser scattering light short-pass (in wavelength) edge filters (EF) with edge at 652 nm (1.90 eV) were used.

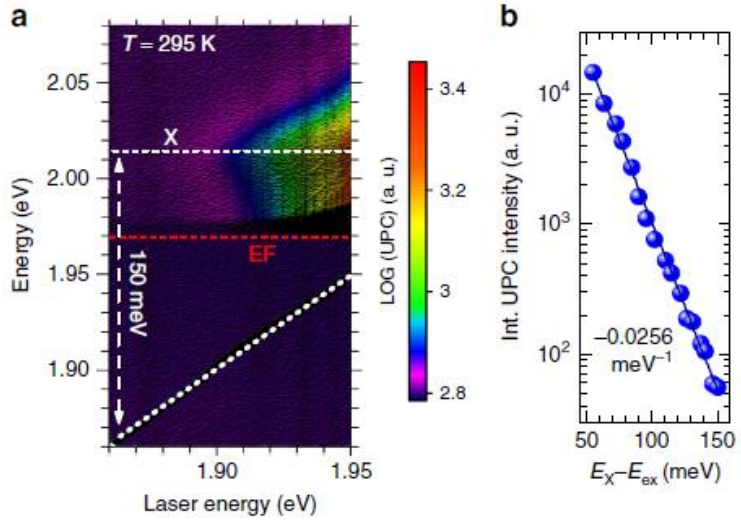

Fig. 2.2 Excitation energy dependence of the upconversion photoemission. (a) Evolution of the upconversion emission spectra as a function of the laser excitation photon energy in WS_2/SiO_2/Si, recorded in ambient, at 295 K. (b) The dependence of the upconversion integrated intensity on the energy difference of the neutral exciton (X) and the excitation photon energy ($E_X–E_{ex}$).

The examples of the upconversion emission spactra in WS_2/SiO_2 and $WS_2/hBN/SiO_2/Si$ structures are shown in Fig. 2.1 (b) and (c), respectively. The intensity of emitted upconverted photons in both $WS_2/SiO_2/Si$ and $WS_2/hBN/SiO_2/Si$ heterostructures strongly correlates with the intensity of normal photoluminescence (PL), spectral shape of which strongly depends on the thickness of hBN layer. This is why, for further studies of the excitonic upconversion photoluminescence in ambient at 295 K, I chose single layers of WS_2 exfoliated on SiO_2/Si substrate, as they exhibit the most prominent emission attributed to the neutral exciton (X). Figure 2.2 (a) shows the colour map of the upconversion photoemission intensity as a function of the exciting photon energy, whereas Fig. 2.2 (b) presents the dependence of the upconversion photoluminescence integrated intensity in the spectral range from 1.91 eV to 2.10 eV on the energy difference ($E_X – E_{ex}$) of the exciton X and the exciting photon energy E_{ex}. For the energy difference $E_X – E_{ex}$ from 50 meV to 155 meV, the integrated upconversion photoluminescence intensity decreases with decreasing excitation photon energy with the rate equal to $-0.0256\ meV^{-1}$.

In order to identify the mechanism responsible for the upconversion in monolayer WS_2, particularly the nature of the initial states being in resonance with the incident photons (~1.85 eV), the comprehensive, temperature –dependent PL experiments of WS_2/SiO_2 and $WS_2/hBNSiO_2/Si$ structures were performed. In contrast to WS_2 monolayers deposited directly on the SiO_2/Si substrate, for all the investigated $WS_2/hBN/SiO_2/Si$ structures the additional emission lines, except the X line, appeared in the PL spectra in ambient, at T = 295 K (see Fig. 2.3 (a)). One of the lines, positioned at the energy of 1.964 eV, 42 meV below that of the exciton (X), is attributed to a trion (T), whereas the lower-energy broad features labeled as L, positioned at ~1.86 meV, are attributed to strongly localized exciton [**23** ,**H6**]. The L lines in the PL of the $WS_2/hBN/SiO_2/Si$ heterostructures are recorded about 150 meV below that of the free exciton. Moreover, for all the $WS_2/hBN/SiO_2/Si$ heterostructures with finite hBN thickness, the characteristic red shift of X line, about 8 meV below its position recorded for the WS_2 monolayer deposited on SiO_2/Si, is observed. This energy difference is related to the change of the exciton-binding energy E_b and the bandgap energy E_g ($E_X = E_g - E_b$). The different dielectric environments of WS_2 monolayers lead to the reduction of both Eg and Eb energies in $WS_2/hBN/SiO_2/Si$ heterostructures in comparison with the $WS_2/SiO_2/Si$ structures. These results show that an extra hBN layer used between the flake and SiO_2/Si substrate can act as a buffer layer and changes the doping level in the monolayer system. Here, it is manifested by the altering trion to exciton emission intensity ratio (T/X) shown in the inset of Fig. 2.3 (a). For normal $WS_2/SiO_2/Si$ structure, the trion peak is hardly detected in the PL spectra, whereas for $WS_2/hBN/SiO_2/Si$ heterostructures with increasing hBN thicknesses the T/X PL intensity ratio increases. The rising value of the T/X PL intensity ratio indicates that the increasing of hBN layer thickness leads to the growth of two-dimensional electron gas concentration in monolayer WS_2. This dependence can be explained by the fact that the WS_2 is naturally n-doped whereas positively charged defects

(or charge inhomogeneity) are embedded in SiO_2 surface, close to the monolayer WS_2. Hence, the positively charge defects in SiO_2 surface strongly influence an electron charge in WS_2. Intuitively, the electron-binding energy to the charged defect embedded in SiO_2 is the largest for $WS_2/SiO_2/Si$ structures and should decrease with increasing thickness of hBN layer. Our experimental results are qualitatively consistent with recent theoretical calculations of the ground-state energies of electrons as a function of the distance of a positive point-charge defect from the mid-plane of the monolayer [**41**].

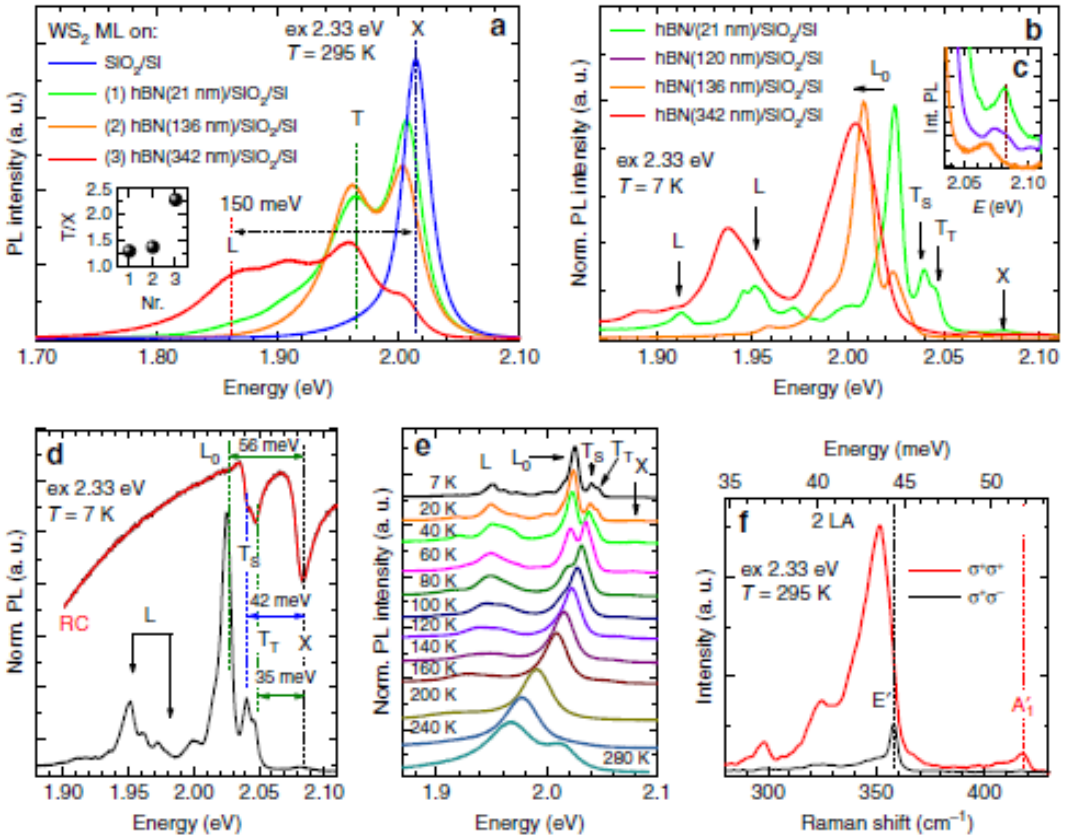

Fig. 2.3 Photoluminescence, reflectance contrast and Raman scattering. (a) Examples of photoluminescence spectra of monolayer WS_2 deposited on SiO_2/Si substrate and on $hBN/SiO_2/Si$ substrates with different thicknesses of hBN layers, excited with incident photon energies of 2.33 eV (532 nm), and recorded in ambient at 295 K. The inset shows the T/X emission intensity ratio for different flakes, 1, 2 and 3, respectively. (b) Examples of photoluminescence spectra of monolayer WS_2 deposited on $hBN/SiO_2/Si$ substrates with different thicknesses of hBN layers, excited with incident photon energies of 2.33 eV (532 nm), and recorded in vacuum at 7 K. (c) The red-shift of neutral exciton (X) emission line for increasing thickness of hBN layer. d The comparison of low temperature PL and RC spectra recorded in $WS_2/hBN(21\ nm)/SiO_2/Si$. (e) The temperature evolution of PL spectra in $WS_2/hBN(21\ nm)/SiO_2/Si$. (f) Helicity-resolved Raman spectra excited with 532 nm laser line for $WS_2/SiO_2/Si$.

These results show that the electron-binding energy is the largest when the defect is at the surface, and it significantly decreases from 150 meV to a few meV as the distance between point-charge defect and the mid-plane of the monolayer exceeds 100 nm. Interestingly, the L lines attributed to localized excitons emerge in the PL spectra on the low energy wing of the trion when hBN layer is placed between the WS_2 monolayer and SiO_2 substrate and they are well resolved in the spectra and comparable with the trion emission for hBN thickness higher than 300 nm.

Figure 2.3 (b) compares low temperature (7 K) spectra, normalized to maximum photoluminescence intensity, detected for selected WS_2/hBN/SiO_2/Si heterostructures with different thicknesses of hBN layers (21 nm, 120 nm, 136 nm), respectively. There is a qualitative correlation between the energy of the peak associated with particular transition and the thickness of the hBN layer. The emission lines detected at higher energies and interpreted as nearly free complexes, including X, T_S, T_T [[**24**, **38**]] and L_0 [**42**, **H6**], exhibit an apparent red shift with increasing thickness of hBN (for X line see Fig. 2. 3(c)), whereas the series of lower energy L lines (strongly localized) remains energetically inert. Moreover, the emission intensity of the L lines differs slightly from flake to flake due to different amount and types of created vacancies and the difference in the local two-dimensional electron gas concentration, but without evident correlation with the thickness of hBN layer. Also, for all the studied samples, the L transitions do play a significant role in absorption type experiments, such as reflectance contrast (RC) spectroscopy. While, it is worth to note, that the extra hBN layer deposited between SiO_2 and WS_2 allows to observe different kind of trions (T_S, T_T i $L_{0)}$, both in the PL and RC spectra (Fig. 2.3 (d)). Furthermore, the temperature evolution of the PL spectra of WS_2/hBN/SiO_2/Si structures, presented in Fig. 2.3 (e), shows that the L lines are detected in the optical spectra up to 160 K, which corresponds to significantly higher temperature range than for standard WS_2/hBN/SiO_2/Si structures. It allowed to observe that at high temperatures the L lines merge energetically with the states from the trion tail.

In order to identify potential phonon modes involved in the upconversion process, the polarization resolved Raman scattering measurements were done at room temperature, under ambient conditions. Figure 2. 3 (f) presents helicity resolved Raman scattering spectra of a monolayer WS_2 deposited on an SiO_2/Si substrate excited with the 532 nm laser line with σ^+ polarized excitation and detection either in σ^+ or σ^- polarization, labeled $\sigma^+\sigma^+$ or $\sigma^+\sigma^-$. This method allows us to resolve and precisely assign degenerate Raman bands for the monolayer WS_2 [**43**], the E' and 2LA (M), respectively. The first order out-of-plane A'_1 mode (52 meV) is visible only in $\sigma^+\sigma^+$ configuration, whereas the in-plane E' (44 meV) is detected only in the spectra of opposite helicity $\sigma^+\sigma^-$.

Since the polarization properties of the A'_1 phonon ($\sigma^+\sigma^+$) are consistent with preservation of valley polarization of the exciton complex for selective excitation with circularly polarized light in TMDs [**7-9**, **38**], I proposed that the upconversion mechanism in WS_2 is based on the coupling between the initial and final excitonic states mediated by the three A'_1 phonons. This scenario was determined by two

aspects : (i) the upconversion energy gain of 150 meV matches the energy of three phonons equals to 156 meV, (ii) the symmetry of the electronic states within the K valleys dictates a stronger interaction with the out-of-plane A'$_1$ phonon than with the in-plane E' mode [**44**, **45**].

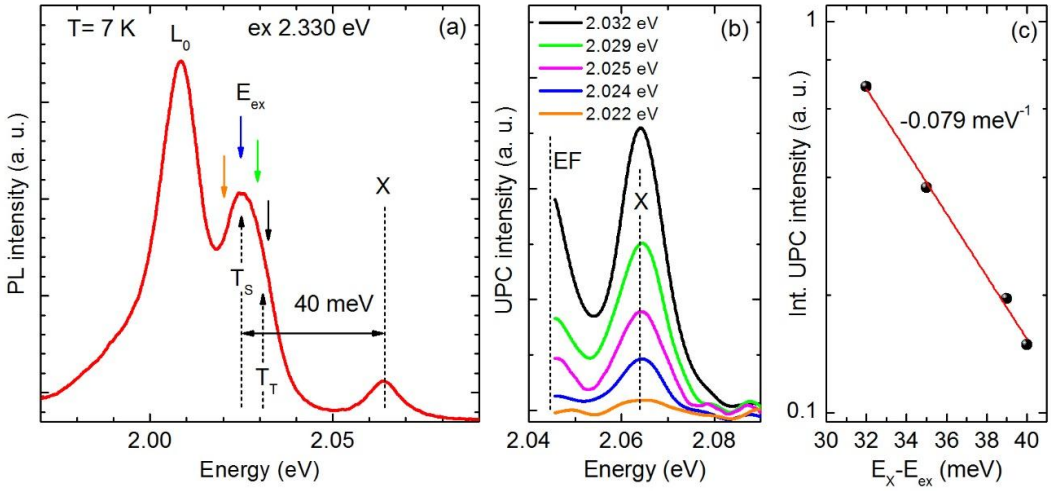

Fig. 2.4 Upconversion photoemission process in monolayer WS_2 at 7 K. (a) The PL spectrum recorded for WS_2/hBN(136 nm)/SiO_2/Si at 7 K. Black, green, blue and orange arrows point out excitation energies used in UPC experiment. (b) Examples of UPC spectra at 7 K excited with energies indicated by coloured arrows in (a). (c) The dependence of the upconversion integrated intensity on the energy difference of the neutral exciton (X) and the excitation photon energy (E_X–E_{ex}).

In order to elucidate the nature of the initial states in the anti- Stokes emission process, I performed complementary upconversion photoluminescence measurements, at low (7 K) and intermediate temperatures (70 K). Then, I considered two scenarios. At room temperature, due to the upconversion energy gain of 150 meV comparable with the energy separation of the X and L, one of the possible explanation is that incident photon is in resonance with an exciton localized on impurity. However, taking into account two aspects: (i) absence of any L features in RC spectra (week absorption on excitons localized on impurities), (ii) the exponential drop of upconversion intensity as excitation energy is lowered from the exciton into the energy gap, I excluded this scenario. Hence, I proposed that the absorption of an incident photons at 295 K is related to the states from the tail of the trion. It was also confirmed by comparative PL and upconversion PL measurements at low and intermediate temperatures.

At T = 7 K (Fig. 2.4 (a)-(c)) the energy gain of upconversion emission amounts to about 42 meV, which is comparable with the energy difference between the X and T_S emission lines (spin singlet trion binding energy plus Fermi level energy) and also nearly resonates with the energy of one optical phonon (A'$_1$ or E'). This suggests that at low temperature the upconversion photoluminescence process is related to the coupling between the trion (T) and exciton (X) states mediated by one optical phonon, as in work of Jones et al. [**38**]. Moreover, for the energy difference

E_X–E_{ex} between 32 meV and 40 meV, the integrated upconversion intensity decreases with decreasing excitation photon energy, with the rate equal to $-0.079\ meV^{-1}$ (Fig. 2.4 (c)), which is about three times higher (in absolute value) than the one estimated at 295 K under ambient condition.(– $0.0256\ meV^{-1}$).

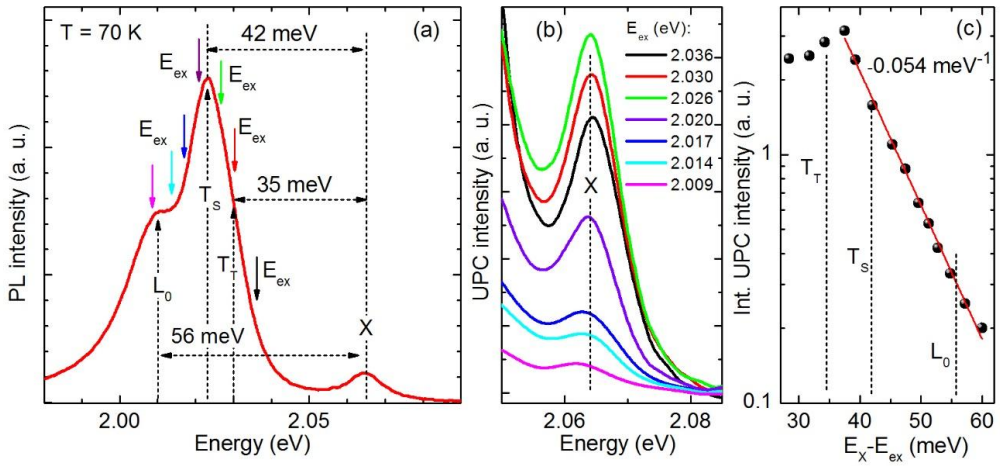

Fig. 2.5 Upconversion photoemission process in monolayer WS_2 at 70 K. (a) The PL spectrum recorded for WS_2/hBN(136 nm)/SiO_2/Si at 70 K. The coloured arrows point out excitation energies used in UPC experiment. (b) Examples of UPC spectra at 70 K excited with energies indicated by coloured arrows in (a). (c) The dependence of the upconversion integrated intensity on the energy difference of the neutral exciton (X) and the excitation photon energy (E_X – E_{ex}).

Figure 2.5 (a) shows the PL spectrum detected at 70 K. Coloured arrows indicate excitation energies (E_{ex}) of the upconversion photoluminescence spectra presented in Fig. 2.5 (b). At this temperature, the exciting photon energy required to achieve a detectable upconversion photoluminescence (gradual intensity growth just above the noise floor) is found to exceed $E_{ex} = 2.009$ eV, which corresponds to the energy position of the L_0 line in the PL spectra. Interestingly, following the upconversion photoluminescence spectra excited at different energies, presented in Fig. 2. 5 (b), it is seen that with decreasing excitation energy from 2.036 to 2.026 eV, the intensity of the upconversion photoluminescence increases and achieves maximum at excitation with energy nearly equals to the energy of the trion in a spin singlet state Ts (green arrow in Fig. 2. 5 (b)). With further decreasing excitation energy, the upconversion photoluminescence decreases and is not detected at excitation energies below 2.009 eV. Figure 2.6 (c) presents the dependence of the integrated intensity of upconversion photoluminescence on the energy difference E_X–E_{ex} of the exciton X and the exciting photon energy E_X. For the energy difference from 37 meV to 60 meV, the integrated upconversion photoluminescence intensity decreases with decreasing excitation photon energy with the rate equal to $-0.054\ meV^{-1}$, which is about two times higher and about one and half times lower (in absolute value) than those estimated under ambient at 295 and 70 K, respectively. Importantly, these results show that upconversion photoluminescence ener-

gy gain increases with increasing temperature. The energy gain of ~60 meV at 70 K suggests that more than one phonon is involved in the upconversion process. Also, the maximum of the upconversion intensity achieved at excitation with energy nearly equals to the energy of the trion T_S confirms that the initial states in the upconversion process are attributed to the trion and states from the tail of the trion at low and high temperatures, respectively.

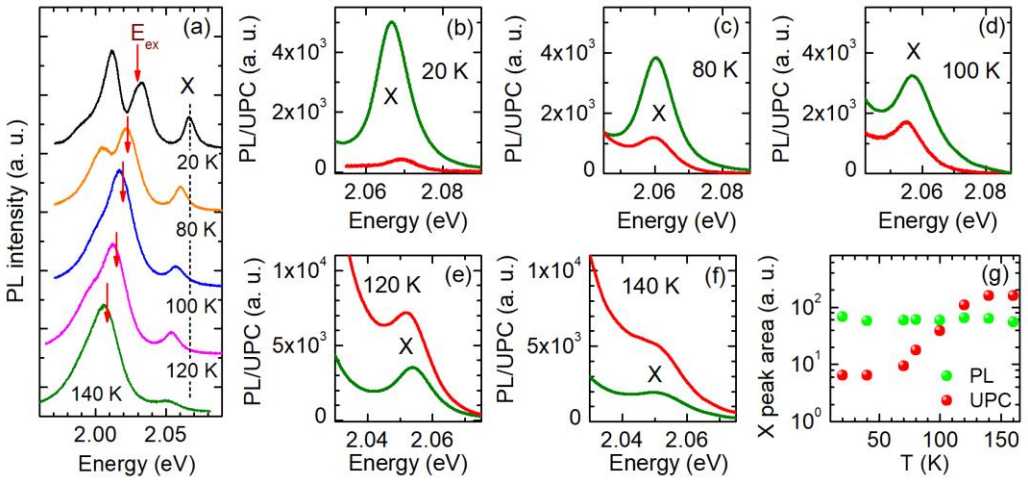

Fig. 2.6 Temperature dependence of upconverted emission with the energy gain of 37 meV. (a) Schematic representation of the experiment: typical PL spectra with indicated by red arrows excitation energies used in UPC measurements at corresponding temperatures. (b)–(f) Examples of normal (green line) and upconversion (red line) photoluminescence spectra (green and red lines, respectively) recorded at 20 K, 80 K, 100 K, 120 K, 140 K, respectively. (g) The normal (green circles) and upconverted (red circles) excitonic photoluminescence integrated intensities as a function of temperature.

In addition, the simultaneous normal and upconversion photoluminescence spectra at temperatures from 20 K to 160 K were performed. At all temperatures, the excitation of the normal photoluminescence was fixed at 2.33 eV, while the excitation energy of the upconversion photoluminescence was tuned in to maintain the constant energy separation between the excitation (E_{ex}) and the exciton emission (E_X). The upconversion experiments were performed for two different energy gains (E_X–E_{ex}) equal to 37 meV (Fig. 2.6) and 87 meV (Fig. 2.7), which are related to one phonon and multi phonon assisted upconversion, respectively. For the energy separation of 37 meV, which nearly matches the energy of the trion (T) emission, I observed that upconversion photoluminescence intensity increases and exceeds standard photoluminescence intensity at 120 K, whereas normal photoluminescence remains nearly constant with increasing temperature. Here, the observed excitonic upconversion growth is governed by increasing phonon population [**38**]. It is also accompanied by simultaneous increase of the trion emission intensity with increasing temperature. While, for the energy gain (E_X–E_{ex}) equal to 87 meV, which corresponds to the energy of the states from the trion tail and slightly ex-

ceeds the energy of localized excitons L, I found consistent intensity increase of X upconversion photoluminescence and nearly constant normal X photoluminescence in temperature range from 100 K to 160 K. However, for the higher energy gain (87 meV), the intensity of X upconversion photoluminescence is relatively lower than the intensity of the normal X photoluminescence at each temperature. Here, the observed excitonic upconversion growth at corresponding temperatures is again attributed to the increasing phonon population and is correlated with simultaneous increase of the trion emission. Additionally, this growth is accompanied by a gradual decrease of the localized excitons PL emission, which confirms that in high temperature multi-phonon upconversion process the incident photon is rather in resonance with the states from the tail of the trion than in resonance with the exciton localized on the impurity.
Moreover, the efficiency of the upconversion photoluminescence process by means of the changes in the exciton emission intensity for different energy gains and gradual intensity descent rates is the highest at room temperature and can be tuned by about two orders of magnitude over the mean energy gain of 100 meV (Fig. 2.2 (b)).

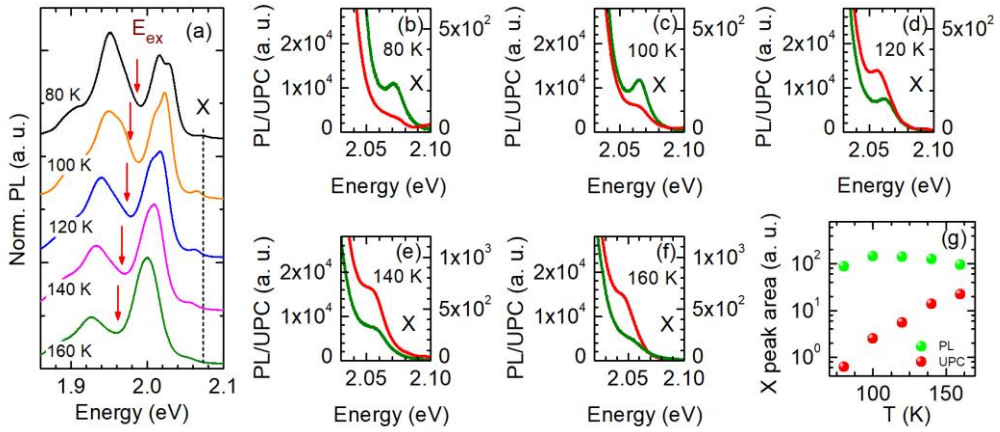

Fig. 2.7 Temperature dependence of upconverted emission with the energy gain of 87 meV. (a) Schematic representation of the experiment: typical PL spectra with indicated by red arrows excitation energies used in UPC measurements at corresponding temperatures. (b)–(f) Examples of normal (green line, left vertical scale) and upconversion (red line, right vertical scale) photoluminescence spectra recorded at 80 K, 100 K, 120 K, 140 K, 160 K, respectively. (g) The normal (green circles) and upconverted (red circles) excitonic photoluminescence integrated intensities as a function of temperature from 80 K to 160 K.

The character of the high temperature upconversion photoluminescence in monolayer WS2 was also was evaluated in the excitation power-dependent measurements, in both ambient (black line) and vacuum (red line) at 295 K (Fig. 2.8 (a) – (b)), with the excitation photon energy of 1.890 eV, corresponding to the broad emission of the localized excitons L (Fig. 2.8). Figure 2.8 (a) presents the comparison of the upconversion PL spectra measured under different condition, for the

same excitation power densities. The upconversion photoluminescence spectra of WS_2 measured in ambient conditions are dominated by the exciton emission X, whereas the trion T is hardly detected in the spectra. In contrast, in vacuum the upconversion photoluminescence spectra clearly resolves emission of both the exciton and trion with comparable intensities. Their energy separation equals to 42 meV, and matches the values reported in previous studies. These results confirm that under ambient conditions the physisorbed O_2 and H_2O molecules deplete n-type materials [**35**, **36**] and the 2D electron concentration is reduced in monolayer WS_2. Figure 2.8 (c) and (d) present typical photoemission spectra recorded for several excitation power densities, in ambient and in vacuum, respectively. Figure 4 (e) shows the total upconversion intensity in ambient (black points) and vacuum (magenta stars) as a function of excitation power density, integrated over the same energy range from 1.9 eV to 2.1 eV. They reveal weak sublinear (0.53) and linear (~1) dependence for increasing excitation power in ambient and in vacuum, respectively. These observation clearly shows that upconversion mechanism strongly depends on 2DEG concentration. Furthermore, as all the data of total upconversion intensities follow the sublinear and linear relationship, we exclude the possibility of nonlinear optical generation of the observed upconversion photoluminescence, such as two-photon excitation-induced emission [**46**] and exciton Auger scattering [**47**].

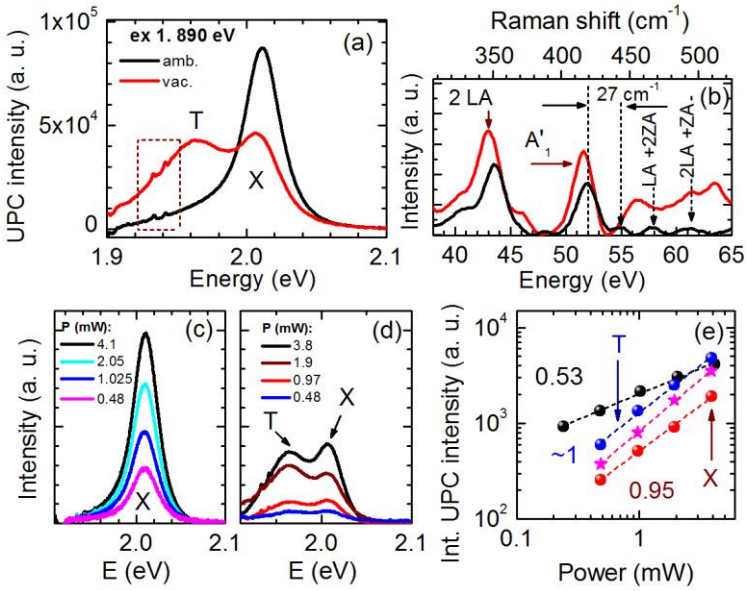

Fig. 2.8 (a) Excitation power dependence of the upconversion photoemission. (a) Comparison of the spectra in monolayer WS_2 deposited on SiO_2/Si substrate, recorded in ambient (black line) and vacuum (red line), excited with the same incident photon energy 1.890 eV and power, at 295 K. (b) Comparison of the anti-Stokes Raman spectra measured in ambient (black line) and vacuum (red line), obtained by subtracting the emission from the corresponding UPC spectra in (a). (c), (d) examples of spectra excited with different laser powers, recorded in ambient and vacuum, respectively. (e) The integrated upconversion photoemission intensity plotted as a function of excitation power density for total spectra recorded in am-

bient (black circles), in vacuum (magenta stars), for X peak in vacuum (red points), for T peak in vacuum (blue point).

3) Optical properties of monolayer $Mo(S_ySe_{1-y})_2$.

The characteristic features of the strictly two dimensional group –VI TMDs [**1 - 12**], such as direct band gaps at $K^{\pm}$ points, valley-contrasting strong spin splitting of the valence and conduction bands and optical properties dominated by robust excitons are also excepted for monolayer ternary alloys such as $M_{1-x}N_xX_2$ (M = Mo, N = W, X = Se, S) lub $M(X_yY_{1-y})_2$ [**48**]. The TMD alloys with controlled composition provide additional tuning possibilities, such as engineering of the optical band-gap and the spin-orbit splitting of the valence and conduction bands, which make them promising candidates for applications.

In the following part of my studies I also focused on the characterization of the optical properties and the lattice dynamics of the ternary $Mo(S_ySe_{1-y})_2$ alloys [**H4, H5, B4**]. The fundamental motivation for these investigations was also related to exciton - phonon interactions in strictly two dimensional system with controlled composition *y*, which allows to tune phonon energy through trion binding energy in order to obtain the resonant condition for observation of the strong increase of exciton - trion coupling mediated by the optical phonon [**38**, **H1**].

In $MoSe_2$ the A'_1 optical phonon energy, 29.8 meV, resonances with the trion binding energy of 30 meV, which in turn corresponds to the exciton – trion separation in photoluminescence spectra. While, in MoS_2 the A'_1 phonon energy of 51 meV strongly exceeds those in $MoSe_2$, and also is greater than the exciton - trion separation in the photoluminescence spectra of MoS_2 monolayer [**H6**]. Hence, even small incorporation of sulfur atoms into $MoSe_2$ host lattice results in significant increase of the (Se-S) A∗ phonon energy with out-of-plane symmetry [**B6, H4, H5**].

Figure 3.1 (a) presents the set of unpolarized Raman spectra of the $Mo(S_ySe_{1-y})_2$ monolayers measured at T = 295 K for the varying composition *y* from 0 to 0.5. For the binary $MoSe_2$, the frequencies of the first-order Raman lines are equal to 240.6 cm^{-1} (29.8 meV) and 286 cm^{-1} (35.4 meV). They are assigned to the out-of-plane A_1 and in-plane E_2 modes, respectively. The presence of a sulfur atom in the host lattice of $MoSe_2$ induces vibrations with out-of-plane weight in the vicinity of A_1 mode, resulting in characteristic splitting into two Raman features denoted as A (Se-Se) and A∗ (Se-S), which evolve in a different manner as a function of increasing S content *y*. The splitting is directly related to the different distribution of the chalcogenide atoms within the $Mo(S_ySe_{1-y})_2$ layers. The A'_1 (Se-Se) vibration corresponding to the Se-Se configuration shifts to lower frequency upon increasing *y*. Also, the intensity of this peak decreases with increasing composition *y*. Moreover, based on the polarization - resolved Raman scattering measurements of the bulk $Mo(S_ySe_{1-y})_2$ alloys, this Raman line disappears from the spectra when the sulfur content exceeds y = 0.5 [**B6**]. While, within mixed A∗ (Se-S) group, we can identify at least three components, shifting to higher frequency upon increasing *y*. They are well resolved for composition 0.1 and 0.2, when the $2Se_2$+ 1SeS,

$2Se_2 + 1S_2$ or $1Se_2+2SeS$ arrangements are the most probable [**B6**]. Furthermore, the Raman studies on bulk crystals [**B6**] show that A* (Se-S) group is detected in the spectra for composition $0 < y < 1$. Both split features Se-Se and Se-S preserve the polarization selection rules of the out-of-plane vibration, originating at the frequency of $MoSe_2$–A_1 mode [**43**]. As seen in Fig. 3.1 (b)- (c) the A_1(Se-Se) and A* (Se-S) modes show up only in $\sigma^+\sigma^+$ configuration, whereas E_2(Se- Se) and E_2(Se-S) are detected only in the spectra of opposite helicity $\sigma^+\sigma^-$.

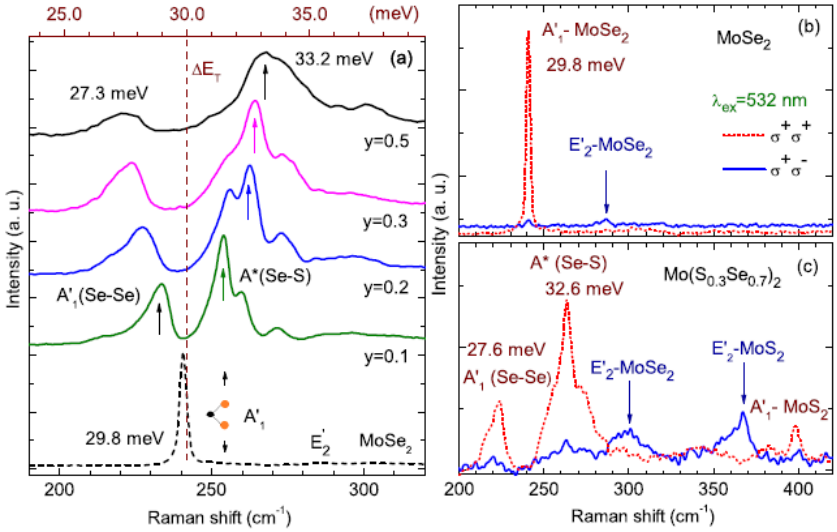

Fig. 3.1 The Raman spectra detected of the studied MLs at T = 295 K. (a) Unpolarized spectra for the binary $MoSe_2$ and ternary $Mo(S_ySe_{1-y})_2$. Helicity-resolved spectra for (b) $MoSe_2$ and (c) $Mo(S_{0.3}Se_{0.7})_2$.

In order to get further information about the impact of the alternating composition *y* on optical properties of the $Mo(S_ySe_{1-y})_2$ monolayers I performed the temperature- dependant, comparative photoluminescence and reflectance contrast measurements (from 7 K to 295 K). In figure 3.2, the examples of comparative PL and RC spectra of the studied MLs for $MoSe_2$, $Mo(S_{0.3}Se_{0.7})_2$, and $Mo(S_{0.5}Se_{0.5})_2$ are presented at two temperatures T = 7 and 120 K. For all samples, two distinct transitions are observed in PL spectra. They are separated by 30 meV and attributed the exciton (X, higher-energy one) and trion (T , lower-energy one) emissions. The common feature observed in PL spectra of all studied MLs is that at low temperatures (below 100 K) the PL intensity of the trion exceeds those of exciton. Interestingly, at T = 120 K in MoS_2 the trion PL intensity is lower than that of exciton, whereas for composition $y = 0.3$ and $y = 0.5$ the trion still dominates the spectra. The complementary Fig. 3.3 (a) –(e) presents temperature dependence of the PL intensity of excitons and trions, and the total PL intensity for all MLs. As seen if Fig 3.3, the PL intensities of X and T lines decrease with increasing temperature but with substantially different rates for different MLs. In contrast to binary $MoSe_2$, where above 120 K the exciton PL intensity slightly exceeds that of trion, for all the ternary samples, at high temperature regime the trion dominates

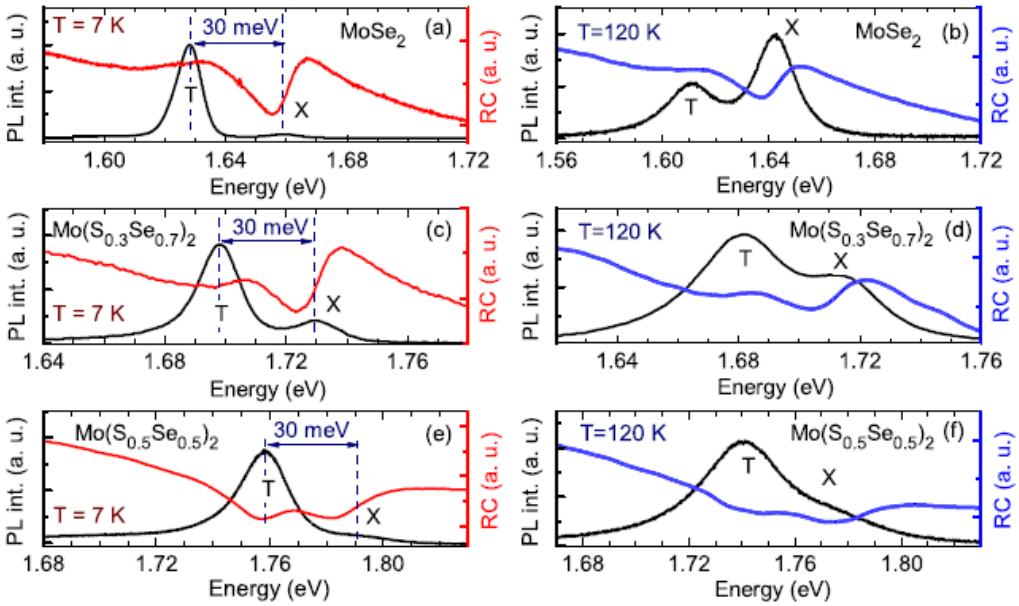

Fig. 3.2 Examples of comparative PL and RC spectra recorded at T = 7 and 120 K for MLs of (a), (b) $MoSe_2$, (c), (d) $Mo(S_{0.3}Se_{0.7})_2$, (e), (f) $Mo(S_{0.5}Se_{0.5})_2$.

in the PL spectra. Interestingly, for composition $y = 0.3$ the PL intensity of X and T decreases as function of the temperature almost with the same rate. Instead, for composition y = 0.5 the PL intensity of T decreases about 4.5 times in temperature range from 7 to 120 K and then it decreases only about 1.4 times in the temperature range from 140 to 295 K, while the PL intensity of X seems to be almost monotonic. These differences are also clearly reflected in Fig. 3.4, which shows the temperature dependence of the trion to exciton PL intensity ratio I_T/I_X in all the studied MLs.

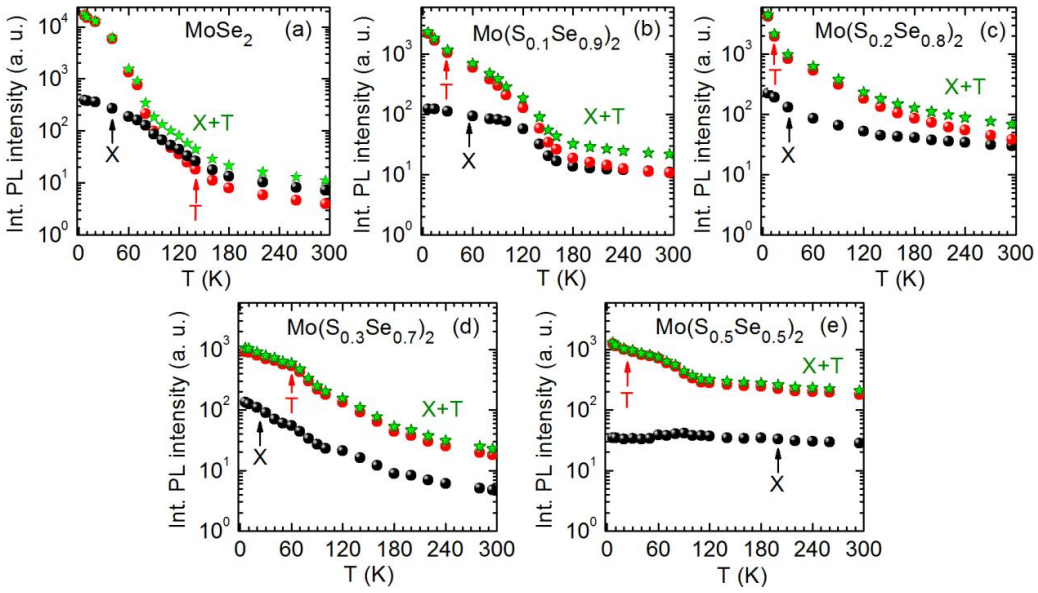

Fig. 3.3 The PL intensities of excitons and trions, and total PL intensity as a function of the temperature in (a) $MoSe_2$, (b) $Mo(S_{0.1}Se_{0.9})_2$, (c) $Mo(S_{0.2}Se_{0.8})_2$, (d) $Mo(S_{0.3}Se_{0.7})_2$, and (e) $Mo(S_{0.5}Se_{0.5})_2$.

At low temperatures, below T ≤ 100 K, the PL intensity of T is much higher than of X for all ternary samples but no evident correlation between I_T/I_X ratio and increase of sulfur content is observed. At higher temperatures T >100 K, the I_T/I_X ratio in ternary $Mo(S_ySe_{1-y})_2$ MLs exceeds those of $MoSe_2$ and increase with the increase of the sulfur mole content. Moreover, the increase of the PL intensity ratio (I_T/I_X) is significantly correlated with the increase of the A∗ (Se-S) phonon energy in $Mo(S_ySe_{1-y})_2$ (see Fig. 3.5).

The strong increase of the trion PL intensity in $Mo(S_ySe_{1-y})_2$ MLs with increase of sulfur mole content to two effects. First, with the increase of sulfur mole content we observe simultaneous increase of the optical phonon energy, from E_{ph} = 29.8 meV to E_{ph} = 33.2 meV, for binary $MoSe_2$ and ternary $Mo(S_{0.5}Se_{0.5})_2$, respectively. This phonon shift likely leads to the stronger exciton - trion coupling mediated by the optical phonon A*, which energy exceeds the trion binding energy (Fig. 3.1 (a)), as in WSe_2 and WS_2 monolayers [**38**, **H1**]. This explanation can be also supported by the data presented in Fig. 3.5, which show that for small sulfur contents $y < 0.3$ the high-temperature trion to exciton PL intensity ratio (I_T/I_X) increases roughly linearly with the increase of the A∗(Se-S) phonon energy.

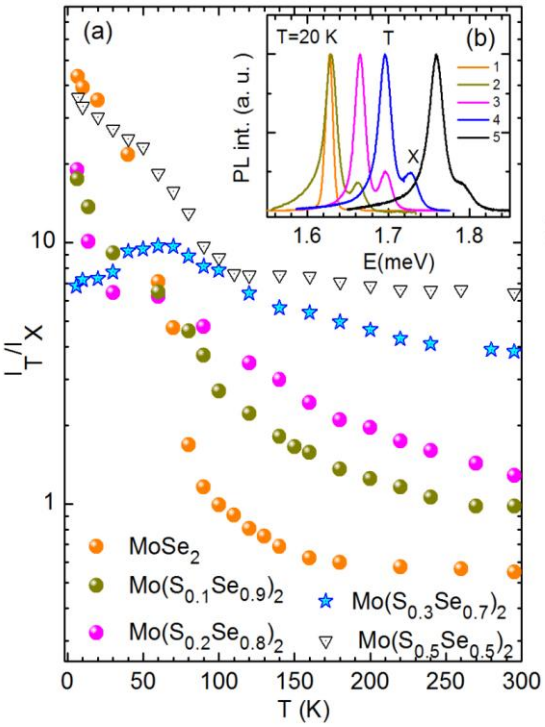

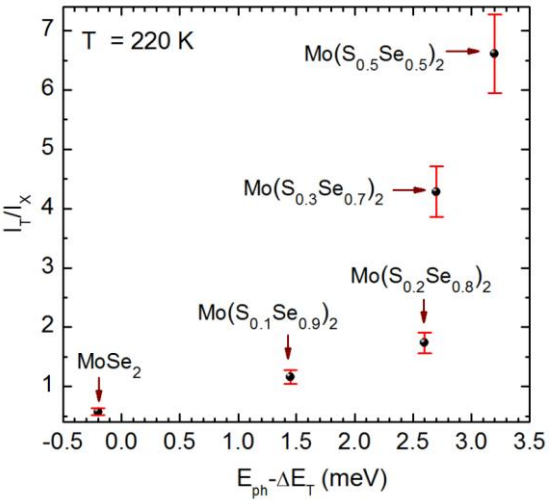

Fig. 3.5 The dependence of the trion to exciton integrated intensity ratio on the energy difference $E_{ph} - \Delta E_T$ at T = 220 K.

Fig. 3.4 The temperature dependence of the trion to exciton PL intensity ratio I_T/I_X in monolayers of $Mo(S_ySe_{1-y})_2$ alloys. In the inset, the PL spectra of all studied samples recorded at T = 20 K are compared: (1) $MoSe_2$, (2) $Mo(S_{0.1}Se_{0.9})_2$, (3) $Mo(S_{0.2}Se_{0.8})_2$, (4) $Mo(S_{0.3}Se_{0.7})_2$, (5) $Mo(S_{0.5}Se_{0.5})_2$.

The second mechanism stabilizing a trion in PL spectra of $Mo(S_ySe_{1-y})$ is related to the increase of the two-dimensional electron gas concentration with increasing sulfur content. It can be seen in Fig. 3.5 as the abrupt increase of I_T/I_X ratio for the higher sulfur content y ≤ 0.3. The increase of the two-dimensional electron gas

concentration in $Mo(S_ySe_{1-y})$ is also manifested in the comparative PL and RC spectra as the relative increase of the optical amplitude of charged complex (Fig. 3.2). Moreover, it is consistent with the substantial difference in the intrinsic two-dimensional electron gas concentration in $MoSe_2$ and MoS_2 monolayers in vacuum [**H6**], which in sulfides is about two orders of magnitude higher than in selenides [**4, 16**].

In order to demonstrate qualitatively the increase of 2DEG concentration with the sulfur mole content, I used again the method of the comparative PL measurements in ambient and vacuum, where the intrinsic two-dimensional electron gas concentration can be reduced and increased, respectively, due to different amount of physisorbed O_2 and H_2O molecules on the flake. Figure 3.5 (a) – (c) shows the comparison of the PL spectra recorded at T = 295 K in ambient and vacuum for (a) $MoSe_2$, (b) $Mo(S_{0.2}Se_{0.8})_2$, and (c) $Mo(S_{0.5}Se_{0.5})_2$. As is seen, under ambient condition for all monolayers, the maximum of PL intensity is detected at the exciton, whereas in vacuum the maximum PL intensity shifts gradually from the exciton in $MoSe_2$ to the trion in $Mo(S_{0.5}Se_{0.5})_2$. This observation indicates the increase of 2DEG concentration with the increase of sulfur mole content in $Mo(S_ySe_{1-y})_2$ MLs placed in vacuum.

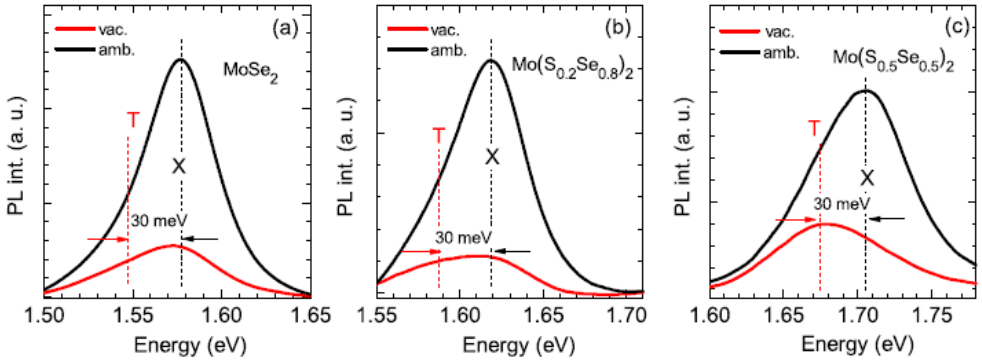

Fig. 3.6 The photoluminescence spectra recorded at T = 295 K in ambient and vacuum for (a) $MoSe_2$, (b) $Mo(S_{0.2}Se_{0.8})_2$, and (c) $Mo(S_{0.5}Se_{0.5})_2$.

4) The study of dispersive 'b'-mode in monolayer MoS_2 in temperature dependent resonant Raman scattering experiments.

The monolayer TMDs are two dimensional systems which are very good platform for studies of fundamental effects based on second – order processes that involves the resonant scattering of excited electrons by phonons in the 2D Brillouin zone [**44, 49**].

The resonant Raman scattering (RRS) is widely used to study the electron-phonon interactions and electronic band structures in semiconductor. The observation of the rich variety of features in the second-order Raman spectrum of TMDC is strongly dependent on the incident photon energy, which covers the energy of the excitonic levels [**49**].

The goal of presented work [**H3**] was to characterize the dispersive 'b'-mode in monolayer MoS_2 in the detailed RRS studies as a function of exciting laser energy and temperature T = 7 -300 K. The investigation were focused mainly on the dependence of the electron- phonon interactions on 2DEG concentration.

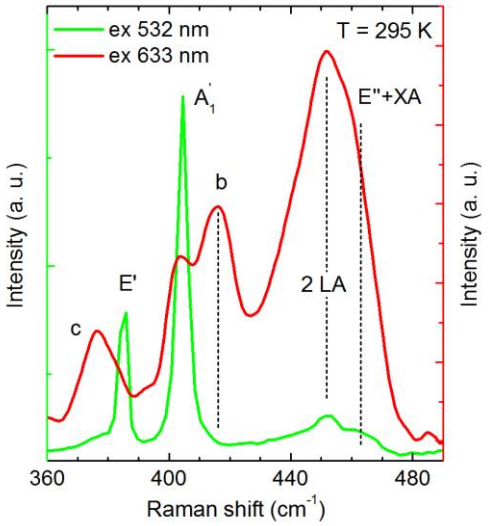

Fig. 4.1 Room temperature of NRRS (532 nm, green) and RRS (633 nm, red) spectra Raman scattering spectra of monolayer MoS_2.

Figure 4.1 presents the comparison of the Raman scattering spectra of monolayer MoS_2 for non-resonant ($\lambda = 532$ nm) and resonant ($\lambda = 632.8$ nm) excitations in the spectral range 360 – 480 cm^{-1}. The non-resonant Raman scattering (NRRS) spectrum of monolayer MoS_2 is dominated by two vibrational modes: E' at 384 cm^{-1} and A'$_1$ at 406 cm^{-1}. Additionally, the week and broad band at 460 cm^{-1} is observed, commonly attributed to the overtone of the LA phonon at the M point in the BZ and assigned to the 2LA(M) band [**49**]. However, Carvalho et al. [**44**] attributed this feature to four different second order scattering processes involving LA phonons near the saddle point between K and M (pDOS singularities) and from LA phonons near ~K and ~M. The RRS (633 nm, 1.96 eV) spectrum of monolayer MoS_2 is more complex. At resonant excitation second-order modes are more intensive than the first-order modes. Also, two additional modes named in literature as *b* and *c* appear in the RRS at 418 cm^{-1} and 378 cm^{-1}, respectively. In the previous studies of bulk MoS_2 the peaks *b* and c were also observed [**50**, **51**]. The peak *c* was assigned to a dispersionless transverse optical phonon E^2_{1u} from the Γ point [**51**], while the *b* mode, with a dispersive behavior near the A and B excitonic resonances, was accessed to the excitonic polariton scattered by successive emission of a dispersive quasi-acoustic interlayer breathing phonon and a dispersionless phonon E^2_{1u}, both along the **c** axis and at Γ point of BZ [**50**]. However, the presence of the 'b' and c modes in RRS spectra of monolayer MoS_2 [**44**, **52**] rules out these interpretations. Livneh and Spanier [**52**] interpreted the *b* band as the double Raman scattering involving combinations of the acoustic LA' and TA' phonons at K points of BZ. This interpretation was confirmed recently by Carvalho et al. [**44**] in the multiple energy excitation Raman study of monolayer

and bulk MoS_2. While, the *c* mode was attributed to the second order process involving phonons from K and M valleys.

In order to gain an insight into the nature of the dispersive *b* mode, the Raman scattering spectra of monolayer MoS_2 as a function of temperature (T = 7–295 K) and the excitation laser energy at resonant conditions were performed. As seen in Fig. 4. 2 (a), for the excitation energy at 1.96 eV, below T = 100 K, the mode *b* is not detected in Raman spectra. However, above 80 K the *b* mode appears in Raman spectra and gradually gains in intensity with the further increase of the temperature. It is strictly correlated with the resonant conditions, when the A exciton energy level crosses the excitation energy. It is clearly seen In Fig. 4.2 (b) which presents temperature evolution of the RC spectra of monolayer MoS_2. At T = 7 K two well resolved resonances are detected in the RC spectra and attributed to the lowest energy bright A-exciton and trion. Due to the high concentration of 2DEG in MoS_2 monolayer, the trion resonance dominates the RC spectra and is well resolved at all measured temperatures, whereas the X resonance is hardly resolved in the RC spectra above T > 160 K [**H4**, **H6**]. With the increase of temperature the X and T resonances in RC spectra shift to lower energy. When the excitation energy (1. 96 eV) exceeds the A exciton energy, the b mode appears and is well resolved in the Raman spectra.

The temperature dependence of the E', A_1' and *b* bands are presented in Fig. 4.2 (c). The absolute values of the temperature coefficients of E', A_1' modes equal 0.4×10^{-2} and 0.8×10^{-2} cm^{-1}/K, respectively. The temperature coefficient of the *b* mode is significantly higher and equal 3.5×10^{-2} cm^{-1}/K. This is due to the fact that the frequency shift of the *b* mode is substantially affected by the change in the position of the exciton energy with respect to the excitation photon energy.

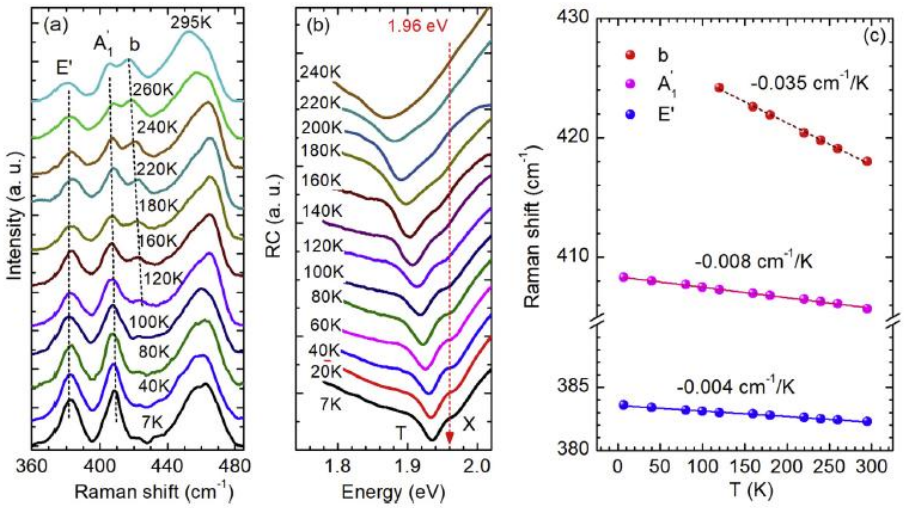

Fig. 4.2 (a) Raman scattering spectra and (b) reflectivity contrast spectra of MoS_2 recorded at T = 7 – 295 K and vacuum. The Raman spectra are excited by a 632.8 nm line of He-Ne laser marked in (b) as a dashed red line. (c) Temperature dependence of observed Raman peak positions.

The dispersion of the *b* mode was also probed in the excitation energy dependant Raman scattering spectra at T = 7 K and vacuum, when the incident photon energy is tuned across the A exciton level (1.964 eV), from 1.9592 eV to 1.9965 eV (Fig. 4.3 (a)). With the laser excitation of the photon energy equals 1.9592 eV and lower than the A exciton energy the *b* mode is not recorded in the Raman spectra. When the incident photon energy is just above the A exciton energy level the *b* line appears at 430 cm^{-1} and shifts to lower frequency to A_1' phonon line. Fig. 4.3 (b) presents the dependence of the frequency shift of the *b* mode as a function of the excitation phonon energy. The frequency shift is almost linear and equal to -83 cm^{-1}/eV.

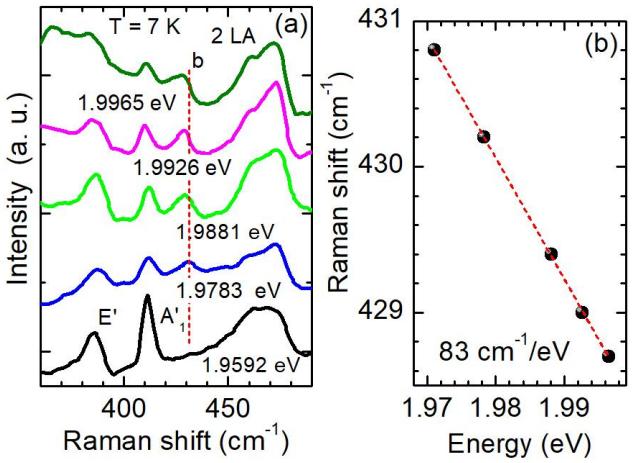

Fig. 4.3 Examples of the Raman scattering spectra of monolayer MoS_2 recorded for various incident photon energies at T = 7 K and vacuum. (b) The evolution of the *b* mode as a function of the incident photon energy.

The similar studies of the Raman scattering spectra of monolayer MoS_2 as a function of the incident phonon energy were performed at room temperature T = 295 K, in ambient (Fig. 4.4 (a) and b)). As at low temperature the energy position of E' and A'$_1$ phonon modes are independent on excitation photon energy, whereas the *b* mode shifts almost linearly to lower frequency with the rate equal to -71 cm^{-1}/eV, close to that at T = 7 K. Interestingly, both the frequency shift of the b mode as a function of the incident photon energy at T = 7 and 295 K, equal -83 and -71 cm^{-1}/eV, respectively, are very close to those obtained in the similar studies of bulk crystals, equal -80 cm^{-1}/eV at T = 7 K [**50**] and almost two times higher than those recently reported by B. R. Carvalho et al. [**44**] for monolayer MoS_2 equal 40 cm^{-1}/eV at T = 295 K.

These significant differences in the dispersion of the *b* mode are likely related to the significantly different two dimensional (2D) electrons gas concentration in the investigated samples. This result also implies a strong dependence of the electron-phonon interaction on 2DEG concentration.

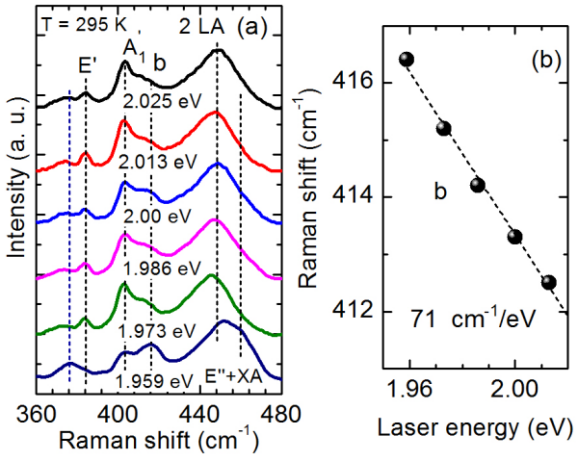

Fig. 4.4 (a) Examples of the Raman scattering spectra of monolayer MoS_2 recorded for various incident photon energies at T = 295 K and vacuum. (b) The evolution of the 'b' mode as a function of the incident photon energy.

5) Exciton binding energy and hydrogenic Rydberg series in layered ReS_2.

Unlike VI- group TMDs, layered ReS_2 crystallizes in a distorted 1 T diamond-chain structure with triclinic symmetry unit cell [**53-55**]. Each layer consists of a sheet of Re atoms located between two S atoms sheets, bound by strong ion-covalent bond between Re and S atoms. The S atoms have a distorted octahedral coordination around the Re atoms which results in the formation of Re−Re chains clusters along the b-axis [**55**]. The distortion of the crystal lattice leads to anisotropic in-plane optical and electrical properties. Additionally, as suggested in the recent Raman scattering studies [**56**], due to in-plane distortion in ReS_2 the interlayer coupling is weak in comparison to VI -group TMDs, which should result in a lack of correlation between the number of layers and the alteration of physical properties in ReS_2. In contrast, recent photoluminescence (PL) and reflectance spectroscopy experiments on bulk, few- and monolayer ReS_2 imply that the transition energies of the observed excitons can be tuned with layer thickness [**57**]. Another controversy is related to the nature of the energy gap of ReS_2. Some authors have argued that ReS_2 exhibits a transition from the indirect to direct optical band gap when thinned from bulk to monolayer [**58**, **59**], similarly as in the group VI TMDCs. However in ref.[**56**, **60]**, the authors have proven the contrary, i.e. that the energy gap in ReS_2 is direct independently of the number of layers.

The aim of the work [**H2**] was to clarify those issues, and to provide insight into the nature of excitons observed in the optical spectra of ReS_2 using the accuracy of low temperature (7 K) photoluminescence, reflectance contrast and excitation photoluminescence experiments. In addition, the magneto-photoluminescence measurements were conducted in the Voigt configuration with magnetic field up to 10 T with a 1 T step applied along the **b** axis (**B**||**b**).

The anisotropy of the optical properties in layered ReS_2 was studied in polarization- resolved photoluminescence and reflectance contrast experiments at 7 K. In the PL studies, the incident light was circularly polarized (σ^+) and incident photon

energy was equal to 2.33 eV. Then, the PL spectra were analyzed in linear polarization configuration with the polarization angle of the electric field light (**E**) varied between 30° and 120° with respect to the Re chain axis (**b**-axis). The results are shown in Fig. 5.1 (a).

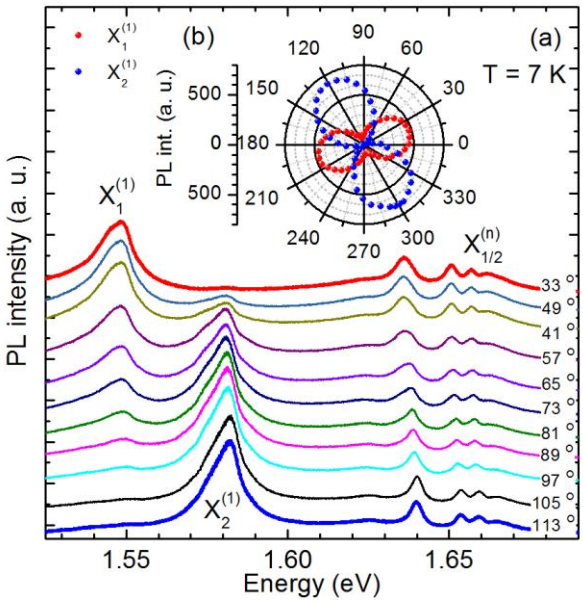

Fig. 5.1 (a) Polarization-resolved photoluminescence spectra, measured at 8° intervals from 30° to 120°. (b) The integrated PL intensity of the $X_1^{(1)}$ and $X_2^{(1)}$ ground states emission plotted as a function of the polarization angle. The data are presented in a polar plot over a 360° range for clarity.

In the low energy sector of the PL spectra shown in Fig. 5.1 (a) two well resolved excitonic peaks are observed, which are attributed to the excitonic ground states 1 s and label as $X_1^{(1)}$ and $X_2^{(1)}$. Their relative PL intensity changes drastically with the polarization angle but the PL maxima of both lines are detected at the same energy independently of the polarization angle. This implies that these excitons are strongly polarized along different directions of the crystal. In the higher energy sector of the PL spectra, next four peaks, labeled in analogy to hydrogenic series as 2 s, 3 s, 4 s and 5 s, are observed and attributed to excited states of the Rydberg series of the excitons $X_1^{(1)}$ and $X_2^{(1)}$. In order to distinguish between the two excitonic series of excited n = 2–5 states, the PL spectra was analysed in two opposite polarizations, where emission of the $X_1^{(1)}$ exciton or the $X_2^{(1)}$ exciton disappears from the spectra. From the detailed analysis of the evolution of total PL intensity of $X_1^{(1)}$ and $X_2^{(1)}$ emission presented in Fig. 5.1 (b), it is found that $X_1^{(1)}$ related peak disappears at 113° (blue line) polarization angle, whereas $X_2^{(1)}$ one at 33° (red line). The same conditions respond to series $X_1^{(n)}$ and $X_2^{(n)}$, respectively. The PL spectra recorded at these two polarizations are presented in Fig. 5.2 (a). The peak positions determined as the maxima in PL spectra are plotted in Fig. 5.2 (b) i (c) as function of the quantum number n, for the excitons X_1 and X_2, respectively.

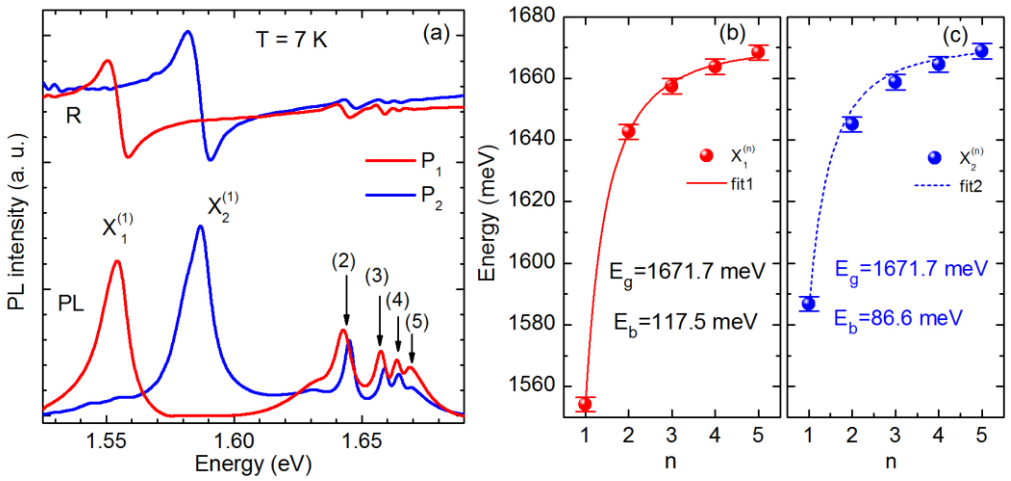

Fig. 5.2 (a) Polarization-resolved PL and RC spectra of bulk ReS_2 recorded in two linear polarization with the angle between **E** and **b** equal to 33° (red line) and 113° (blue line). (b) and (c) Experimentally and theoretically obtained transition energies for the 3D exciton states as a function of the quantum number n, for the X_1 and X_2 excitons, respectively.

In order to calculate the exciton binding energies of X_1 and X_2 excitons, the experimental data were compared with theoretical prediction of hydrogenic Rydberg series. Accordingly, the formula typically employed for the description of three dimensional (3D) Wannier excitons in inorganic semiconductors was used [**61**]: $E^{(n)}_b = E_g - R^*_y/n^2$, where E_g is the energy gap, n is the number of exciton state, $E_b^{(n)}$ is the binding energy at nth excitonic state and Ry* is the effective Rydberg constant. Moreover, to estimate the binding energy of X_1 and X_2 excitons according above model, it was assumed that both excitons are related to the same energy gap E_g, as predicted in recent numerical calculation [**62**]. The estimated energy gap was equal to 1671.7 meV, while the Coulomb binding energies of excitons X_1 and X_2 were equal to 117.5 and 86.6 meV, respectively. Then, the relative Bohr radius of X_1 and X_2 excitons was calculated using the well know relations for hydronic like excitons :$E_b/R^*_y = m_{ex}/\varepsilon^2$ i $a_{ex}/a_H = \varepsilon/m_{ex}$, where: $R_y = 13.6$ eV and $a_H = 0.53$ A are Rydberg constant and Bohr radius of the hydrogen atom, respectively; m_{ex} is a relative effective mass of an exciton, ε is the relative dielectric constant of ReS_2 and a_{ex} is the exciton Bohr radius. The relative effective masses of X_1 and X_2 excitons ($1/m_{ex} = 1/m_e + 1/m_h$) equal to $0.33m_e$ i $0.39m_e$, respectively, were calculated using the tensor of the electron and hole effective masses taken from literature [**60**, **63**]. The two dielectric constants in directions along and perpendicular to **b** axis were obtained: $\varepsilon_1 = 6.2$ i $\varepsilon_2 = 7.8$. The estimated exciton Bohr radius was equal to ~1 nm for both excitons.

To strengthen the interpretation of lines attributed to excited states of the Rydberg series of the excitons $X_1^{(1)}$ and $X_2^{(1)}$, the additional photoluminescence excitation measurements at T = 1.8 K were performed. Figure 5. 3 (a) presents polarized 113° PL and 113° PLE spectra in which only the Rydberg series of the exciton X_2 is detected. The PLE signal was detected in the energy range related to the ground

exciton state from 1535 to 1605 meV (marked by dotted line). The laser excitation energy was tuned across the energy of the excited states 2 s, 3 s, 4 s and 5 s from 1619 to 1676 meV (the energy region of excitation of PLE signal is marked by arrows). The PLE signal is presented in Fig. 5. 3 (b) as a color map. The comparison of the PLE and PL spectra is displayed in Fig. 5.3 (b) and (c), respectively, and shows that features observed in the PLE spectra correspond to the energy position of the emission lines in the relevant energy regions of PL spectra. This result confirms that high energy lines observed in the PL spectra are indeed related to the hydrogenic Rydberg series of X_1 and X_2 excitons.

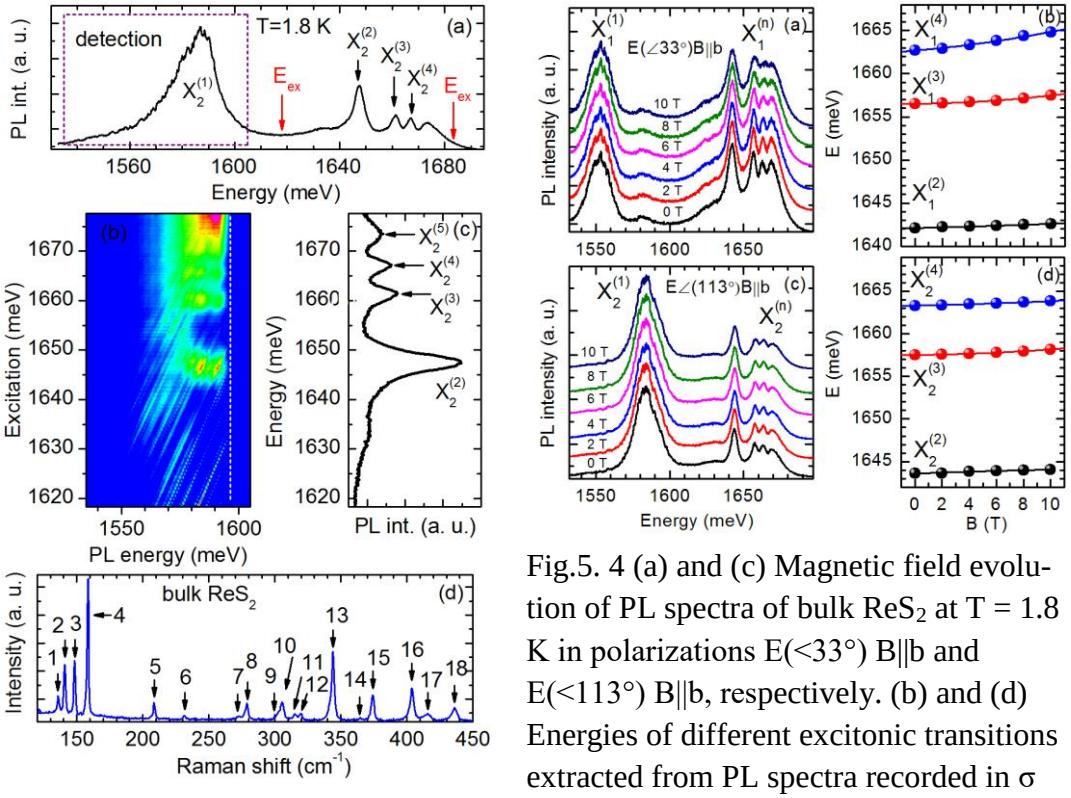

Fig.5. 4 (a) and (c) Magnetic field evolution of PL spectra of bulk ReS_2 at T = 1.8 K in polarizations E(<33°) B||b and E(<113°) B||b, respectively. (b) and (d) Energies of different excitonic transitions extracted from PL spectra recorded in σ and π polarizations, respectively.

Rys .5. 3 (a) The PL and PLE spectra of bulk ReS_2 recorded at T = 1.8 K.(a) The 113° PL spectrum. The energy regions of detection and excitation of PLE signal are marked by dotted lines and arrows, respectively. (b) The 113° PLE signal plotted as a color map. Red and blue color indicate high and low intensity, respectively. (c) The 113° PL spectrum presented in the energy region of PLE signal. (d) Unpolarized Raman spectra of bulk ReS_2.

Moreover, for the laser excitation energy lower than energy of the 2s excited state, no emission is detected and the features observed in the low energy sector of 113° PLE spectra are related to Raman active optical phonons. For comparison, Fig. 5. 3 (d) shows the non-resonant (2.33 eV), unpolarized Raman scattering spectra of bulk ReS_2. In the 120–450 cm^{-1} range we can distinguish up to 18 phonon modes (marked by arrows) whose energies agree well with the previous studies of Raman spectra of ReS_2 [**56, 64**].

The magneto-photoluminescence measurements have been conducted in the Voigt [**65**] configuration with magnetic field up to 10 T with a 1 T step applied along the **b** axis (**B**||**b**). In Fig. 5. 4 (a) and (c) the PL spectra recorded in the magnetic fields from 0 to 10 T with a 2 T step are presented for two distinctive linear polarizations (**E**(33°)**B**||**b**) and (**E**(113°)**B**||**b**) (as in Fig. 3a), respectively. The magnetic shift of all the observed lines (ΔE) is very small. For the ground states of the excitons X_1 and X_2 the shift is not measurable, whereas for the excited states it is less than 2 meV for the highest applied magnetic field B = 10 T. This observation mainly confirms the strong Coulomb binding of the both excitons. Due to the large width of emission lines (full widths at half maximum (FWHM) equal to ~15 meV and ~7 meV for the ground and excited states of X_1 and X_2 excitons, respectively) the Zeeman splitting is not observed the accurate estimation of the Lande g factor is not possible.

Further optical spectroscopy investigations were performed on ReS_2 flakes with different thicknesses. The thickness of the flakes was determined by atomic force microscope. Figure 5. 5 (a) presents unpolarized PL spectra of ReS_2 flakes with different number of layers (from 8L to 1L). For all the studied flakes in the low energy sector of PL spectra two emission lines are detected, which by comparison to PL spectra of bulk crystals were attributed to optical transitions of the ground states of excitons X_1 and X_2. However, in contrast to bulk ReS_2 crystals, the excited states of excitons X_1 and X_2 in the PL or RC spectra were not resolved. At the higher energy, there was only the broad PL feature (marked as ExS in Fig. 5.5 (a)), which energy position increased when the thickness was thinned down to monolayer. Moreover, as in the bulk ReS_2 crystal, the excitons X_1 and X_2 are strongly polarized in emission and pseudo-absorption spectra (Fig. 5.5 (b)). However, the total PL intensity of both excitons strongly increases with the number of layers, and starts to saturate for flakes thicker than 8 layers, which is seen in Fig. 5.5 (a). This is in contrast to the behavior observed in the group VI TMDCs, such as MoS_2, $MoSe_2$, WS_2 and WSe_2, where the PL intensity of the monolayer increases by orders of magnitude due to the crossover from an indirect band gap in the bulk to a direct band gap in the monolayer [**1-12**].

Moreover, the decreasing PL intensity for thinner samples implies that in layered ReS_2 the direct band gap occurs at the Γ-point of the Brillouin zone irrespective of the crystal thickness. Hence, the oscillator strength of excitonic transitions should increase simultaneously for thicker samples. As seen in Fig. 5.5 (d), with decrease of the number of layers, from 15 L to 1 L, both X_1 and X_2 excitons exhibit strong blue shift, which is 114 meV and 146 meV, respectively. Simultaneously, their relative energy separation increases from 30 meV to 60 meV, as shown in Fig. 5.5 (c). These large shifts are in strong contrast to other, well known group VI TMDCs, where the shifts for the ground state A excitons are much smaller and are in the order of tens meV [**19**]. It is likely due to the stronger electron-hole coupling at Γ-point than at K-point, where direct band gap occurs for the monolayer MoS_2, MeS_2, WS_2 and WSe_2. In the case of group VI TMDCs, an increasing band gap with decreasing flake thickness compensates the effect of an increasing

excitonic binding energy resulting in a weak dependence of exciton transition energy on the layer thickness. In ReS_2, observed increase of the exciton transition energy caused by quantum confinement is less compensated (Fig. 5.5 (d)). Moreover, this energy change is different for excitons X_1 and X_2 likely due to induced in-plane anisotropy.

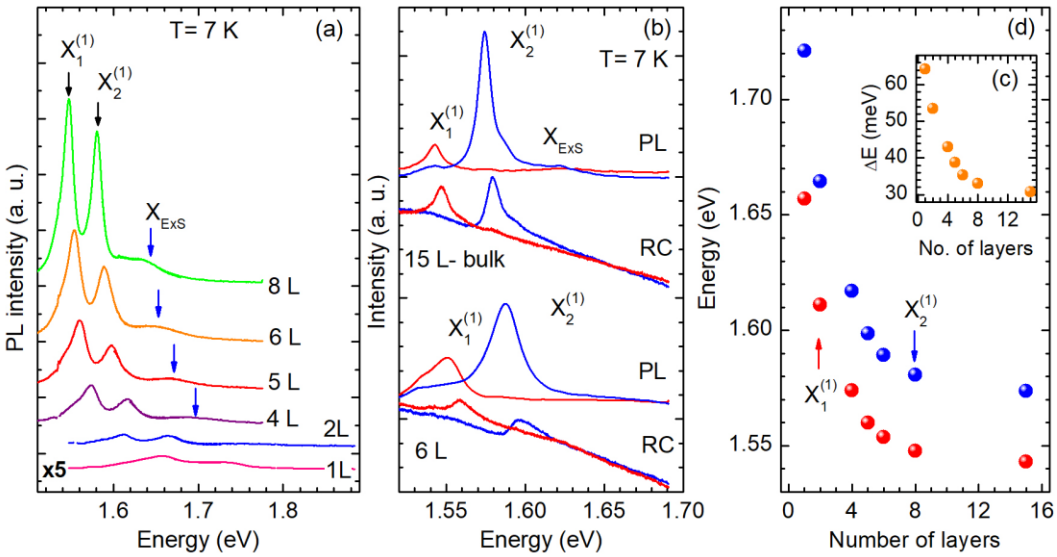

Fig .5.5 (a) Unpolarized PL spectra of 1 L, 2 L, 4 L, 5 L, 6 L and 8 L ReS_2 flakes. (b) Polarization-resolved PL and RC spectra of 15 L and 6 L flakes recorded in two linear polarization with the angle between **E** and **b** equal to 33° (red line) and 113° (blue line). (c) Energies of different excitonic transitions extracted from PL measurements. (d) The transition energy for X_1 and X_2 caused by quantum confinement.

Summary of the achievements

Presented achievements concern both the scientific research and organizational aspects. I built original experimental set- up for optical spectroscopy of low dimensional structures from the ground up. This system allowed me to conduct the simultaneous and comparative photoluminescence (PL), excitation photoluminescence (PLE), pseudo- absorption (reflectance contrast RC)) and Raman scattering measurements with a micrometric spatial resolution in broad temperature range from 7 K to 300 K. For the low temperature optical measurements I set a low vibration closed- cycle cryostat using helium gas. I developed also methods of monolayer separation using mechanical exfoliation techniques with different adhesion tapes, which allowed me to deposit monolayer TMDs on the same SiO_2/Si or hBN/SiO_2/Si substrates. Then, I compared the optical properties of different monolayer TMDs under ambient and vacuum. I focused my research mainly on the studies of many- body effects, in particular the electron – electron and electron – phonon interactions. On the base of experimental results I analyzed all the observed excitonic complexes and I interpreted them in terms of their binding energies, total charge (neutral and charged complexes) [**H4, H5, H6**],

form of localization (nearly free and strongly localized on the defects) **[H6]** and spin – valley configuration of the constituent carriers (intra- and inter-valley singlet and triplet trions) [**H6**].

The significant result in presented studies concerned the observation of additional excitonic resonance in RC spectra of monolayer WS_2, positioned at low energy in respect to the singlet intra-valley trion T_S. This resonance was interpreted as arising from negative trion with electrons located in different valleys, but in the upper conduction bands, forming an electron singlet state [**H6**]. According to my knowledge, it was the first observation of such a feature in the RC spectra of monolayer WS_2. By taking an advantage of the probing simultaneous RC and PL spectra, I observed that energy position of this resonance in RC spectra matches the energy position of emission line in PL spectra, interpreted in the literature as a biexciton (XX). Based on this observation, I proposed an alternative interpretation of the XX line as related to the superposition of: defect bound exciton, trion and biexciton emission [**H6**]. In my studies I emphasized that simultaneous observation of all the excitonic complexes (particularly in WS_2) requires different experimental conditions, including different 2DCG concentration and different quality of the studied samples (highly or low defected). Currently, in the literature there is another interpretation of this prominent feature suggested that it arises from the exciton – plazmon interaction [**66**]. This aspect is still an open question and requires further investigations.

In my studies I focused also on exciton – phonon interaction. In the PL and Raman scattering investigations I showed, that the binding energy of an additional electron to the neutral exciton (trion binding energy) is comparable with a phonon energy (A'_1 or E'). Then, I demonstrated that strong increase of trion PL intensity with the increase of sulfur mole content up to $y \leq 0.5$ in ternary $Mo(S_ySe_{1-y})_2$ is attributed to two effects: (i) strong increase of exciton - trion coupling mediated by the optical phonon, which is realized by tuning phonon energy through trion binding energy, and (ii) significant increase of two-dimensional electron gas concentration [**H4, H5**]. Furthermore, I showed that strong exciton – phonon coupling in monolayer TMDs leads to the high energy, multi- phonon upconversion photoluminescence, which may be used in the optical cooling [**H1**]. In the reverse PL measurements in monolayer WS_2 deposited on SiO_2/Si nad hBN/SiO_2/Si substrates, I showed that upconversion photoluminescence energy gain is up to 150 meV at T = 295 K and 42 meV at T = 7 K. The mechanism of the observed process was interpreted as a strong trion – exciton coupling (also including states from the trion tail) mediated by one and many phonons at low and high temperatures, respectively. According to my knowledge, it was the first observation of the multi-phonon upconversion photoluminescence in the 2D TMDs in ambient and vacuum, demonstrating strong dependence of this process on the 2DEG gas concentration [**H1**]. The strong impact of 2D carrier concentration on the electron- phonon interaction was also probed in the resonant Raman scattering measurements in monolayer MoS_2. I showed that energy dispersion of *b* mode strongly depends on 2DEG concentration, which was tuned by the change of environmental conditions. In addition, I confirmed that it is the second order scattering process involving combinations of the acoustic LA and TA phonons at K points of BZ [**H3**].

The interesting part of my research was also devoted to the layered group- VII TMDs with reduced symmetry such as ReS_2, which crystallizes in a distorted 1 T diamond-chain structure with triclinic symmetry unit cell and possesses the in-plane anisotropy of the optical properties. In these studies I explained the nature of excitons observed in the optical spectra of ReS_2 crystals with different thickness using the accuracy of low temperature (7 K) photoluminescence, reflectance contrast and excitation photoluminescence experiments [**H2**]. Based on the experimental results I proposed that the observed optical transitions arise from two Rydberg series of Wannier excitons. The comparison of the experimental data with theoretical model allowed to calculate: (1) the energy gap equals to 1611 meV, (2) the binding energies of X_1 and X_2 excitons equal to 117.5 meV and 86.6 meV, respectively, (3) the exciton Bohr radius equal to ~1 nm for both X_1 and X_2 excitons, which is comparable with the monolayer thickness and (4) the dielectric constants in directions along and perpendicular to **b** axis equal to $\varepsilon_1 = 6.2$ and $\varepsilon_2 = 7.8$. Furthermore, based on the evolution of PL spectra as a function of number of layer I showed that the total PL intensity of both excitons strongly decreases with the decreasing thickness. The decreasing oscillator strength of excitonic transitions implies that in layered ReS_2 the direct band gap occurs at the Γ-point of the Brillouin zone irrespective of the crystal thickness. This is in contrast to the behavior observed in the group VI TMDCs, where the PL intensity of the monolayer increases by orders of magnitude due to the crossover from an indirect band gap in the bulk to a direct band gap in the monolayer.

5. Discussion of other scientific achievements.

Scientific achievements that do not directly constitute the habilitation achievement and are obtained after doctoral thesis concern the studies of low dimensional semiconducting structures and can be divided into three groups: (a) the studies of the optical properties of two dimensional GaAs/$Al_xGa_{1-x}As$ quantum wells (QW), with different width and doping profile, confining a 2D hole gas [**I1**, **I3**], (b) the studies of the optical properties of AlAs/GaAs core –shell nanowires [**I2**] ,(c) the studies of the optical properties and lattice dynamics of monolayer VI- group TMDs [**B1-B6**].

Two dimensional GaAs/$Al_xGa_{1-x}As$ quantum wells.

After doctoral thesis I continued the optical spectroscopy studies in high magnetic fields (B =17 T) and low temperatures (2-30 K), which were focused on the many –body effects in two dimensional (2D) systems confining charge carriers.

The most important results obtained for 2D GaAs QW are: (1) the observation of a clear correlation between the localization degree of various excitonic complexes (X, X^+, AX^-) and the corresponding values of valence hole g- factor [**I3**], (2) the observation of three distinct dissociation processes for hole cyclotron replica of positive trions bound to neutral acceptors in the spin-doublet state ($SU–A^0X^+_d$) in temperature dependant (2 K to 30 K) PL studies at high magnetic fields B = 17 T [**I1**].

From the polarization-resolved high-field magneto-photoluminescence spectra of asymmetric GaAs quantum wells I determined the spin splitting and corresponding valence hole g-factors of various (neutral and charged) excitonic complexes. By comparing the experimentally obtained values with the theoretical calculation of the real 2D structure (theoretical calculation performed by Arkadiusz Wójs, Krzysztof Ryczko and Maciej Kubisa), I found a clear correlation between the localization degree of various excitonic complexes (X, X^+, AX^-) and the corresponding values of valence hole g- factor. The values of g_h determined for nearly free states, such as neutral exciton (X) and positively charged exciton X^+ demonstrate rather distinct behavior, in terms of both magnitude and magnetic field evolution. The g_h of X was smaller than g_h of X^+ in the entire range of applied magnetic fields (0 – 23 T). At high magnetic fields (23 T) the values of g – factors were equal to 0.88 and 1.55 for X and X^+, respectively. Moreover, the measured g_h of X was in line with the calculated g- factor of excited hole levels of a light hole character (which envelope function extend over the entire QW width.), while g_h of X^+ was approximately equal to an average between ground and excited hole states, suggesting balanced contribution from the ground and excited hole states.

For negatively charged complexes AX^- (A^- + h +e) observed in the low energy range of PL spectra, the hole g- factor begun from a high value at zero field and rapidly decreased with the field growth. Also, g_h increased with the AX- emission energy, from 6 to 11, at B = 0 T, which reflects a significant dependence of these values on the A-/QW distance and penetration of the exciton envelope function into the barrier.

Based on the studies of magnetic field and temperature dependence of PL spectra of superior quality GaAs/$Al_xGa_{1-x}As$ 15 nm wide quantum wells confining a 2D hole gas, I described the thermal dissociation processes of the excitonic complexes, both nearly free and bound on neutral acceptors. At a magnetic field B = 15 T, from the temperature (2- 14 K) decrease of the integrated emission intensity of the hole cyclotron replica of the positive trion bound to the neutral acceptor in the hole spin doublet state (SU- $AX_d^+ = A^- + 3h + e$), the three distinct dissociation processes were observed with the activation energies E_1 = 0.8 meV, E_2 = 1 meV and E_3 = 2.4 meV. Comparing these values with the energy position of particular emission lines in PL spectra, I found that the activation energies E_1 and E_2 are related to dissociations resulting in a free hole (h) and an exciton bound to a neutral acceptor in the hole spin-singlet (A^0X_s) or triplet state (A^0X_t). The third activation energy E_3 was attributed to the dissociation into a free positive trion X^+ and a neutral acceptor (A^0).

In addition, from the temperature evolution of the integrated emission of the free trion lines (X^+) I evaluated the transition energy between the two triplet trion states, the dark one (X^+_{td}) and the bright one (X^+_{tb}), which was equal to ΔE = 0.28 meV and comparable with the difference of the spectral positions of the relevant radiative recombination lines in PL spectra.

The GaAs/AlAs nanowires

The main result obtained for the GaAs- AlAs core- shell nanowires (NWs) concerned resonant coupling between two -dimensional hole gas and optical phonons.

In optical studies of the single core- shell NWs with 60 nm GaAs core, I showed that a modulation of the shell - structure leads to an unintentional p-type doping and formation of a high density two-dimensional hole gas at the core(GaAs)/shell(AlAs) interface. I showed, that placing a narrow 1 nm GaAs quantum well in the AlAs shell effectively getters residual carbon acceptors and hence acts as an efficient impurity trap due to the higher solubility of carbon atoms in GaAs and due to the floating of carbon atoms at the AlAs vacuum interface during the MBE growth. The localization of two – dimensional gas at the core/shell interface of the NW was also confirmed in self-consistent calculation of the charge distribution in NW (M. Royo, A. Bertoni, G. Goldoni, Institute for Nanoscience, CNR-NANO S3, Modena, Italy).
The power and temperature dependant PL measurements of single core – multishell NWs confirmed the two- dimensional character of confined carriers which were involved into radiative recombination (the emission lines in the PL spectra at energies above energy gap of bulk GaAs, E_g = 1.519 eV). In addition, the PL in high magnetic field showed a clear signature of avoided crossings of the n= 0 Landau level emission line with the n = 2 Landau level TO phonon replica. The coupling was caused by the resonant hole-phonon interaction, which points to a large two-dimensional hole density in the structure.

The semiconducting group VI transition metal dichalcogenides.

My research of the optical properties and lattice dynamics of two dimensional group VI TMDs were initiated by characterization of a single WS_2 layers obtained by exfoliation n- type bulk crystals and deposited on standard SiO_2/Si substrate [**B6**]. The aim of this work was to study the nature of optical transitions in monolayer WS_2 using two beam excitation with energies above (2.330 eV) and below (1.44 eV) the band gap. According to my knowledge, this was among the first investigations concerning TMDs, in which the excess density of electrons in the sample was tuned optically, by independent excitation of donor states positioned a few hundreds meV below the conduction band. However, the results showed that low temperature (4 K) PL spectra of n –type WS_2/SiO_2/Si structure is dominated rather by excitons localized on defects (L), independently on the excitation, and the observation of nearly free excitons and trions requires a special, more careful sample preparation. This aspect was continued and presented in my further works directly related to the subject of scientific achievement [**H1**, **H6**].

Simultaneously, I carried out studies on the fundamental physical properties of bulk ternary molybdenum based compounds with formula $Mo(S_ySe_{1-y})_2$ [**B3**, **B4**]. I focused on the impact of composition variations *y* on the lattice dynamics and optical properties. The most important result obtained for mixed $Mo(S_ySe_{1-y})_2$ crystals was observation and explanation of an effect related to the splitting of A_{1g} mode into two groups of modes, A_{1g}(Se-Se) and A*(Se-S), respectively, for increasing *y* composition ($y \leq 1$). Particular Raman lines were attributed to different varying configurations of Se and S atoms around Mo atoms for trigonal pyramidal geometry [**B5**]. The composition evo-

lution of particular modes in the polarization- resolved Raman spectra was compared with a calculation model prediction. It was tri-atomic linear chain model which assumed that interaction between the next nearest neighbors are described by force constants depended on composition *y*. Additionally, the scanning transmission electron microscopy (STEM) imaging (National Institute of Advanced Industrial Science and Technology (AIST), Tsukuba, Japan)) of mixed crystals $Mo(S_ySe_{1-y})_2$ revealed a random arrangement of the S and Se atoms around the Mo atoms and also showed that hexagonal atomic structure is preserved in entire range of composition *y*.
The temperature dependence of the spectral features in the vicinity of the direct band edge (A and B excitons) of mixed-crystals $Mo(S_ySe_{1-y})_2$ solid solutions was measured in the temperature range of 25-295 K by using piezo-reflectance (PzR) [**B3**]. The near band-edge excitonic transition energies were found to vary smoothly with the increase of S content y, indicating that the natures of the direct band edges of $Mo(S_ySe_{1-y})_2$ solid solutions are similar. The energy splitting between the A and B excitons as a function of increasing composition *y* revealed almost linear variation from 253 to 204 meV for $Mo(S_ySe_{1-y})_2$ with $0< x < 1$. These results provide useful information for $Mo(S_ySe_{1-y})_2$ based device applications.
Simultaneously, I participated in research concerning point defects in 2D TMDs and their impact on the properties of the material. In work [**B3**] using scanning TEM (STEM) experiments, a new class of point defects in single-layer TMDs were observed. These defects occur exist in chalcogen-deficient TMDs and can be created through 60° rotations of metal–chalcogen bonds in the trigonal prismatic lattice. By sequential rotations of metal–chalcogen (M–X) bonds, the rotational defects can expand in size and also migrate in the lattice. First-principles calculations provided insights into the evolution of rotational defects and showed that they give rise to p-type doping and local magnetic moments. This result seems to be promising for application since shows that a controllable introduction of rotational defects can be used to engineer the properties of these materials.

In work [**B1**], comparative studies of the optical and electrical properties of one and a few layers of MoS_2 deposited on different substrates, such as SiO_2/Si and aluminum and also for suspended layers (reduced sample –substrate), were conducted. Analyzing a spectral shape of the PL spectra recorded in ambient for monolayer MoS_2 and then following the relative trion to exciton emission intensity ratio (I_T/I_X), the doping in the different monolayer systems was compared and qualitatively determined. The rising value of (I_T/I_X) PL intensity ratio indicted the simultaneous increase of two dimensional electron gas concentration (2DEG) in the studied MoS_2 flakes, which was the highest in MoS_2/SiO_2 structure, then significantly lower in suspended flake and the lowest in monolayer MoS_2 supported on Al. The optical spectroscopy studies of different MoS_2 flakes were qualitatively consistent with KPFM measurements. There was a clear correlation between the increasing value of work function of 4.84 eV, 4.88 eV, 4.98 eV determined for SiO_2/Si supported, suspended and Al supported MoS_2 monolayers, respectively, and the decreasing electron gas concentration determined by the decreasing T/X PL intensity ratio, correspondingly. These results confirmed that

work function is very sensitive to the doping level at the surface of the MoS_2 flakes.

While, in work [**B2**] the complementary study of dispersive *b* mode in monolayer MoS_2 in polarization-resolved resonant Raman scattering experiments were conducted. The Raman spectra were recorded in two polarization configurations labeled $\sigma^+\sigma^+$ or $\sigma^+\sigma^-$ corresponding to the laser line with σ^+ polarized excitation and detection either in σ^+ or σ^- polarization. The first order out-of-plane A'_1 mode was visible only in $\sigma^+\sigma^+$ configuration, whereas the *b* mode was detected only in the spectra of opposite helicity $\sigma^+\sigma^-$. This confirmed that *b* mode is a combination of LA and TA phonons at K points of BZ.

Currently, I continue studies of the optical properties of strictly two dimensional TMDs. In the Polish – German Beethoven project, which I supervise, I do research focused on the spin and pseudospin properties of energetically controllable dark and bright excitons in tailored $Mo_{1-x}W_xSe_2$ alloys.

To sum up my scientific achievements (the full list is included in the annex):
- I am a co-author of 30 peer-reviewed scientific papers in international journals (16 published after PhD), including two articles in Nature Communications, one article in Nano Letters, one article in Scientific Reports. six articles in Physical Review B, one article in Applied Physics Letters, two articles in Nanotechnology, three articles in Journal of Applied Physics and one article in Solid State Communications,
- The total number of citations of my works according to the Web of Science database (as of March 29, 2019) is: 289,
- The number of citations without self-citations is 256,
- The Hirsch index according to the Web of Science database is 8.
- I am doing reviews for international scientific journals, including Applied Physics Letters, Journal of Alloys and Compounds, Solid State Communications, Coatings MDPI, Materials MDPI,
- I participated in over 12 scientific conferences, I delivered 14 talks, including 6 invited oral presentations,
- I am a member of Polish Physical Society,
- I manage one research project (funded by the National Science Center), I was a scientific investigator in three other projects.

List of publications (selection):
Own work directly (B) related to the subject of scientific achievement (obtained after the PhD thesis):

[**B1**] M. Tamulewicz; J. Kutrowska-Girzycka, K. Gajewski, J. Serafińczuk; A. Sierakowski, **J. Jadczak**, L. Bryja,T. Gotszalk, *Layer number dependence of the work function and optical properties of single and few layers MoS2: effect of substrate*, Nanotechnology, **https://doi.org/10.1088/1361-6528/ab0caf**, **IF 3.404**.

[**B2**] J. Kutrowska-Girzycka, P. Kapuściński, **J. Jadczak** and L. Bryja, *The study of dispersive 'b' mode in monolayer MoS_2 in polarization-resolved resonant Raman scattering experiments*, Acta Physica Polonica A **134**, 4 (2018) , **IF: 0.857**

[**B3**] Yung-Chang Lin, Torbjörn Björkman, Hannu-Pekka Komsa, Po-Yuan Teng, Chao-Hui Yeh, Fei-Sheng Huang, Kuan-Hung Lin, **Joanna Jadczak**, Ying-Sheng Huang, Po-Wen Chiu, Arkady V. Krasheninnikov & Kazu Suenaga, *Three-fold rotational defects in two-dimensional transition metal dichalcogenides*, Nature Communications volume **6**, Article number: 6736 (2015), **IF: 11.329**

[**B4**] Y. J. Wu , Po-Hung Wu , **J. Jadczak** , Ching-Hwa Ho, Hung-Pin Hsu , Kuang-Kiao Tiong, *Piezoreflectance study of near band edge excitonic-transitions of mixed-layered crystal $Mo(S_xSe_{1-x})_2$ solid solutions*, Journal of Applied Physics **115**, 223508 (2014), **IF 2.183**

[**B5**] **J. Jadczak**, D. O. Dumcenco, Y. S. Huang,Y. C. Lin, K. Suenaga, P. H. Wu, H. P. Hsu, and K. K. Tiong, *Composition dependent lattice dynamics in MoS_xSe_{2-x} alloys*, Journal of Applied Physics, Volume 116, 193505 (2014), **IF 2.183**

[B6] A. A. Mitioglu, P. Plochocka, **J. N. Jadczak**, W. Escoffier, J. A. Rikken, L. Kulyuk, and D. K. Maude, *Optical manipulation of the exciton charge state in single-layer tungsten disulfide* **,** Phys. Rev. B **88**, 245403 (2013)**, IF 3.664**

Own other work (I), not related to the subject of scientific achievement (obtained after the PhD degree):

[I1] L. Bryja, **J. Jadczak**, K. Ryczko, M. Kubisa, J. Misiewicz, A. Wójs, F. Liu, D. R. Yakovlev, M. Bayer, C. A. Nicoll, I. Farrer, D. A. Ritchie, *Thermal dissociation of free and acceptor-bound positive trions from magnetophotoluminescence studies of high quality $GaAs/Al_xGa_{1-x}As$ quantum wells*, Phys. Rev. B **93**, 165303 (2016), **IF 3.836**

[I2] J. Jadczak, P. Plochocka, A. Mitioglu, I. Breslavetz, M. Royo, A. Bertoni, G. Goldoni, T. Smolenski, P. Kossacki, A. Kretinin, Hadas Shtrikman, and D. K. Maude, *Unintentional high-density p-type modulation doping of a GaAs/AlAs core–multishell nanowire*, Nano Lett. **14**, 2807 (2014), **IF: 13.592**

[I3] J. Jadczak, L. Bryja, K. Ryczko, M. Kubisa, A. Wójs, M. Potemski, F. Liu, D. R. Yakovlev, M. Bayer, C. A. Nicoll, I. Farrer, D. A. Ritchie, *High magnetic field studies of charged exciton localization in $GaAs/Al_xGa_{1-x}As$ quantum wells*, Appl. Phys. Lett. **105**, 112104 (2014), **IF: 3.302**

References:

[1] K. F. Mak, C. Lee, J. Hone, J. Shan and T. F.Heinz, *Atomically thin MoS_2: a new direct-gap semiconductor*, Phys. Rev. Lett. 105 136805 (2010)

[**2**] A. Splendiani et al., *Emerging photoluminescence in monolayer MoS_2*, Nano Lett. 10 1271–5 (2010)

[**3**] G. Eda, H. Yamaguchi, D. Voiry, T. Fujita, M. Chen and M. Chhowalla, *Photoluminescence from chemically exfoliated MoS_2*, Nano Lett. 11 5111–6 (2011)

[**4**] B. Radisavljevic, A. Radenovic, J. Brivio, V. Giacometti and A. Kis, *Single-layer MoS_2 transistors*, Nat. Nanotechnol. 6 147–50 (2011)
[**5**] Y. Zhang et al., *Direct observation of the transition from indirect to direct bandgap in atomically thin epitaxial $MoSe_2$*, Nat. Nanotechnol. 9 111–5 (2014)
[**6**] D. Xiao, G. B. Liu, W. Feng, X. Xu and W. Yao, *Coupled spin and valley physics in monolayers of MoS_2 and other group VI dichalcogenides*, Phys. Rev. Lett. 108 196802 (2012)
[**7**] T. Cao et al., *Valley-selective circular dichroism in MoS_2*, Nat. Commun. 3 887 (2012)
[**8**] G. Sallen et al., *Robust optical emission polarization in MoS_2 monolayers through selective valley excitation*, Phys. Rev. B 86 081301 (2012)
[**9**] K. F. Mak, K. L. He, J. Shan and T. F. Heinz, *Control of valley polarization in monolayer MoS_2 by optical helicity*, Nat. Nanotechnol. 7 494–8 (2012)
[**10**] Q. H. Wang, K. Kalantar-Zadeh, A. Kis, J. N. Coleman and M. S. Strano, *Electronics and optoelectronics of two dimensional transition metal dichalcogenides*, Nat. Nanotechnol. 7 699–712 (2012)
[**11**] X. Xu, D. Xiao, T. F. Heinz and W. Yao, *Spin and pseudospins in layered transition metal dichalcogenides*, Nat. Phys. 10 343–50 (2014)
[**12**] Y. J. Zhang, T. Oka, R. Suzuki, J. T. Ye and Y. Iwasa, *Electrically switchable chiral light-emitting transistor*, Science 344 725–8 (2014)
[**13**] K. He, N. Kumar, L. Zhao, Z. Wang, K. F. Mak, H. Zhao and J. Shan, *Tightly bound excitons in monolayer WSe_2*, Phys. Rev. Lett. 113 026803 (2014)
[**14**] A. Chernikov, T. C. Berkelbach, H. M. Hill, A. Rigosi, Y. Li, O. B. Aslan, D. R. Reichman, M. S. Hybertsen and T. F. Heinz, *Exciton binding energy and nonhydrogenic Rydberg series in monolayer WS_2*, Phys. Rev. Lett. 113 076802 (2014)
[**15**] Z. Ye, T. Cao, K. O'Brien, H. Zhu, X. Yin, Y. Wang, S. G. Louie and X. Zhang, *Probing excitonic dark states in single-layer tungsten disulphide*, Nature 513 214–8 (2014)
[**16**] J. S. Ross et al., *Electrical control of neutral and charged excitons in a monolayer semiconductor*, Nat. Commun. 4 1474 (2013)
[**17**] F. Withers et al., *WSe_2 light-emitting tunneling transistors with enhanced brightness at room temperature*, Nano Lett. 15 8223–8 (2015)
[**18**] G. Wang, L. Bouet, D. Lagarde, M. Vidal, A. Balocchi, X. Marie Amand, and B. Urbaszek, *Valley dynamics probed through charged and neutral exciton emission in monolayer WSe_2*, Phys. Rev. B 90 075413 (2014)
[**19**] A. Arora, M. Koperski, K. Nogajewski, J. Marcus, C. Faugeras and M. Potemski, *Exciton band structure in layered WSe_2: from a monolayer to the bulk limit*, Nanoscale 7 10421–9 (2015)
[**20**] G. Wang, E. Palleau, T Amand, S. Tongay, X. Marie and B. Urbaszek, *Polarization and time-resolved photoluminescence spectroscopy of excitons in $MoSe_2$ monolayers*, Appl. Phys. Lett. 106 112101 (2015)
[**21**] T. Godde et al, *Exciton and trion dynamics in atomically thin $MoSe_2$ and WSe2: effect of localization*, Phys. Rev. B 94 165301 (2016)

[**22**] K. F. Mak, K. He, C. Lee, G. H. Lee, J. Hone, T. F. Heinz and J. Shan, *Tightly bound trions in monolayer MoS_2*, Nat. Mater. 12 207–11 (2013)
[**23**] G. Plechinger, P. Nagler, J. Kraus, N. Paradiso, C. Strunk, C. Schüller and T. Korn, *Identification of excitons, trions and biexcitons in single-layer WS_2*, Phys. Status Solidi 9 457–61 (2015)
[**24**] G. Plechinger et al, *Trion fine structure and coupled spin–valley dynamics in monolayer tungsten disulfide*, Nat. Commun. 7 12715 (2016)
[**25**] Y. You, X. X. Zhang, T. C. Berkelbach, M. S. Hybertsen, D. R. Reichman and T. F. Heinz, *Observation of biexcitons in monolayer WSe_2*, Nat. Phys. 11 477–81 (2015)
[**26**] A. M. Jones et al, *Optical generation of excitonic valley coherence in monolayer WSe_2*, Nat. Nanotechnol. 8 634–8 (2013)
[**27**] M. Molas, C. Faugeras, A. O. Slobodeniuk, K. Nogajewski, M. Bartos, D. M. Basko and M. Potemski, *Brightening of dark excitons in monolayers of semiconducting transition metal dichalcogenides*, 2D Mater. 4 021003 (2017)
[**28**] Z. Y. Zhu, Y. C. Cheng and U. Schwingenschlogl, *Giant spin-orbit-induced spin splitting in two-dimensional transition-metal dichalcogenide semiconductors*, Phys. Rev. 84 153402 (2011)
[**29**] H. Dery and Y. Song Y, *Polarization analysis of excitons in monolayer and bilayer transition-metal dichalcogenides*, Phys. Rev. B 92 125431 (2015)
[**30**] H. P. Komsa and A. V. Krasheninnikov, *Native defects in bulk and monolayer MoS_2 from first principles*, Phys. Rev. B 91 125304 (2015)
[**31**] A. Gladysiewicz, L. Bryja, A. Wójs and M. Potemski, *Effect of free carriers and impurities on the density of states and optical spectra of two-dimensional magnetoexcitons*, Phys.Rev. B 74 115332 (2006)
[**32**] B. Ganchev, N. Drummond, I. Aleiner and V. Falko V, *Three particle complexes in two-dimensional semiconductors*, Phys. Rev. Lett. 114 107401 (2015)
[**33**] Schmidt T and Lischka K, *Excitation-power dependence of the near-band-edge photoluminescence of semiconductors*, Phys. Rev. B 45 8989 (1992)
[**34**] T. Taguchi, J. Shirafuji and Y. Inuishi, *Excitonic emission in cadmium telluride*, Phys. Status Solidi B 68 727 (1975)
[**35**] S. Tongay, J. Zhou, C. Ataca, J. Liu, J. S. Kang, T. S. Matthews, L. You, J. Li, J. C. Grossman and J. Wu, *Broad-range modulation of light emission in two-dimensional semiconductors by molecular physisorption gating*, Nano Lett. 13 2831–6 (2013)
[**36**] B. Miller, E. Parzinger, A. Vernickel, A. W. Holleitner and U. Wurstbauer, *Photogating of mono- and few-layer MoS_2*, Appl. Phys. Lett. 106 122103 (2015)
[**37**] T. Cheiwchanchamnangij and W. R. L. Lambrecht, *Quasiparticle band structure calculation of monolayer, bilayer, and bulk MoS_2*, Phys. Rev. B 85 205302 (2012)
[**38**] A. M Jones,. et al., *Excitonic luminescence upconversion in a two-dimensional semiconductor*, Nat. Phys. 12, 323–327 (2016)
[**39**] M. Manca et al., *Enabling Valley selective exciton scattering in monolayer WSe_2 through upconversion*, Nat. Commun. 8, 1–7 (2017)
[**40**] P. Tonndorf, R. Schmidt, P. Böttger, X. Zhang, J. Börner, A. Liebig, M. Albrecht, C. Kloc, O. Gordan, D. R. T. Zahn, S. M. de Vasconcellos, and R. Bratschitsch, *Pho-*

toluminescence emission and Raman response of monolayer MoS_2, $MoSe_2$, and WSe_2, Opt. Express 21, 4908 (2013).
[**41**] D. V. Tuan, A. M. Jones, M. Yang, X. Xu, and H. Dery, *Virtual trions in the photoluminescence of monolayer transition-metal dichalcogenides*, Preprint at https://arxiv.org/abs/1805.08722 (2018)
[**42**] M. R. Molas, et al., *The optical response of monolayer, few-layer and bulk tungsten disulfide*, Nanoscale 9, 13128–13141 (2017)
[**43**] S. Y. Chen, C. Zheng, M. S. Fuhrer, & J. Yan, *Helicity-resolved Raman scattering of MoS_2, $MoSe_2$, WS_2, and WSe_2 atomic layers*, Nano. Lett. 15, 2526–2532 (2015).
[**44**] B. R. Carvalho, L. M. Malard, J. M. Alves, C. Fantini, C & M. A. Pimenta, *Symmetry-Dependent Exciton-Phonon Coupling in 2D and Bulk MoS_2 Observed by Resonance Raman Scattering*, Phys. Rev. Lett. 114, 136403 (2015)
[**45**] B. Chakraborty et al., *Symmetry-dependent phonon renormalization in monolayer MoS_2 transistor*, Phys. Rev. B 85, 2–5 (2012)
[**46**] G. Wanget al., *Giant enhancement of the optical second-harmonic emission of WSe2 monolayers by laser excitation at exciton resonances*, Phys. Rev. Lett. 114, 1–6 (2015).
[**47**] S. Mouri et al., *Nonlinear photoluminescence in atomically thin layered WSe_2 arising from diffusion-assisted exciton-exciton annihilation*, Phys. Rev. B 90, 155449 (2014).
[**48**] J. Kang et al., *Monolayer semiconducting transition metal dichalcogenide alloys: Stability and band bowing*, J. Appl. Phys. 113, 143703 (2013)
[**49**] J. Maultzsch, S. Reich, et al., *Double-resonant Raman scattering in graphite: Interference effects, selection rules, and phonon dispersion*, Phys. Rev. B 70 155403 (2004)
[**50**] T. Sekine, K. Uchinokura et al., *Dispersive Raman Mode of Layered Compound 2H-MoS2 under the Resonant Condition*, J. Phys. Soc. Jpn. 53 811–818 (1984)
[**51**] T. Livneh, E. Sterer, *Resonant Raman scattering at exciton states tuned by pressure and temperature in 2H-MoS_2*, Phys. Rev. B 81 195209 (2010)
[**52**] T. Livneh, J.E. Spanier, 2D Mater. 2 35003 (2015)
[**53**]. J. C. Wildervanck, & F. Jellinek, *The dichalcogenides of technetium and rhenium*, J. Less-Common Met.24, 73–81 (1971).
[**54**]. N. Alcock, & A. Kjekshus, *The Crystal Structure of $ReSe_2$*, Acta Chem Scand (1965).
[**55**]. H. J. Lamfers, A. Meetsma, G. A. Wiegers & J. L. de Boer, *The crystal structure of some rhenium and technetium dichalcogenides*, J. Alloys Compd.241, 34–39 (1996).
[**56**] S. Tongay et al., *Monolayer behaviour in bulk ReS_2 due to electronic and vibrational decoupling*, Nat. Commun.5, 3252 (2014).
[**57**] O. Aslan Burak, D. A. Chenet, A. M. van der Zande, J. C. Hone & T. F. Heinz, *Linearly Polarized Excitons in Single-and Few-Layer ReS_2 Crystals*, ACS Photonics3, 96–101 (2015).
[**58**] M. Gehlmann et al., *Direct Observation of the Band Gap Transition in Atomically Thin ReS_2*, Nano Lett.17, 5187–5192 (2017).

[**59**] I. Gutierrez-Lezama, B. A. Reddy, N. Ubrig & A. F. Morpurgo, *Electroluminescence from indirect band gap semiconductor ReS_2*, 2D Mater. 3 (2016).
[**60**] J. L. Webb et al., *Electronic band structure of ReS_2 by high-resolution angle-resolved photoemission spectroscopy*, Phys. Rev. B96, 115205 (2017)
[**61**] C. Klingshirn, *Semiconductor optics* (Springer-Verlag Berlin Heidelberg 2005).
[**62**] J. P. Echeverry & I. C. Gerber, *Theoretical investigations of the anisotropic optical properties of distorted 1 T ReS_2 and $ReSe_2$ monolayers, bilayers, and in the bulk limit*, Phys. Rev. B97, 75123 (2018).
[**63**] D. Ovchinnikov et al., *Disorder engineering and conductivity dome in ReS2 with electrolyte gating*, Nat. Commun.7, 1–7 (2016).
[**64**] Y. Feng et al., *Raman vibrational spectra of bulk to monolayer ReS_2 with lower symmetry*, Phys. Rev. B92, 1–6 (2015).
[**65**] N. Miura, *Physics of Semiconductors in High Magnetic Fields*, (Oxford University Press 2008)
[**66**] D. H. Tuan et al., *Probing many-body interactions in monolayer transition-metal dichalcogenides*, Phys. Rev. B 99, 085301 (2019)